PLOS ONE

RESEARCH ARTICLE

Influence of APOE Genotype on Hippocampal Atrophy over Time - An N=1925 Surface-Based ADNI Study

Bolun Li[1], Jie Shi[1], Boris A. Gutman[2], Leslie C. Baxter[3], Paul M. Thompson[2], Richard J. Caselli[4], Yalin Wang[1]*, Alzheimer's Disease Neuroimaging Initiative[¶]

1 School of Computing, Informatics, and Decision Systems Engineering, Arizona State University, Tempe, Arizona, United Stated of America, **2** Imaging Genetics Center, Institute for Neuroimaging and Informatics, University of Southern California, Marina del Rey, California, United Stated of America, **3** Human Brain Imaging Laboratory, Barrow Neurological Institute, Phoenix, Arizona, United Stated of America, **4** Department of Neurology, Mayo Clinic Arizona, Scottsdale, Arizona, United Stated of America

¶ Membership of the Alzheimer's Disease Neuroimaging Initiative is provided in the Acknowledgments.
* ylwang@asu.edu

OPEN ACCESS

Citation: Li B, Shi J, Gutman BA, Baxter LC, Thompson PM, Caselli RJ, et al. (2016) Influence of APOE Genotype on Hippocampal Atrophy over Time - An N=1925 Surface-Based ADNI Study. PLoS ONE 11(4): e0152901. doi:10.1371/journal.pone.0152901

Editor: Ornit Chiba-Falek, Duke University, UNITED STATES

Received: September 8, 2015

Accepted: March 21, 2016

Published: April 11, 2016

Data Availability Statement: All brain images and demographic information were obtained from the Alzheimer's Disease Neuroimaging Initiative (ADNI) database (adni.loni.usc.edu) and are public and freely accessible.

Funding: This work was funded by the National Institute on Aging (R21AG043760 to BL, JS, LCB, RJC and YW, R21AG049216 to JS, PMT and YW, R01AG031581 and P30AG19610 to RJC), the National Science Foundation (DMS-1413417, IIS-1421165 to YW), and the Arizona Alzheimer's Consortium (ADHS14-052688 to BL, JS and YW). BAG, PMT and YW are also supported, in part, by the

Abstract

The apolipoprotein E (APOE) e4 genotype is a powerful risk factor for late-onset Alzheimer's disease (AD). In the Alzheimer's Disease Neuroimaging Initiative (ADNI) cohort, we previously reported significant baseline structural differences in APOE e4 carriers relative to non-carriers, involving the left hippocampus more than the right—a difference more pronounced in e4 homozygotes than heterozygotes. We now examine the longitudinal effects of APOE genotype on hippocampal morphometry at 6-, 12- and 24-months, in the ADNI cohort. We employed a new automated surface registration system based on conformal geometry and tensor-based morphometry. Among different hippocampal surfaces, we computed high-order correspondences, using a novel inverse-consistent surface-based fluid registration method and multivariate statistics consisting of multivariate tensor-based morphometry (mTBM) and radial distance. At each time point, using Hotelling's T^2 test, we found significant morphological deformation in APOE e4 carriers relative to non-carriers in the full cohort as well as in the non-demented (pooled MCI and control) subjects at each follow-up interval. In the complete ADNI cohort, we found greater atrophy of the left hippocampus than the right, and this asymmetry was more pronounced in e4 homozygotes than heterozygotes. These findings, combined with our earlier investigations, demonstrate an e4 dose effect on accelerated hippocampal atrophy, and support the enrichment of prevention trial cohorts with e4 carriers.

Introduction

Alzheimer's disease (AD) is the most common cause of dementia, accounting for 60–80% of cases [1, 2]. Effective presymptomatic diagnosis and treatment of AD could have enormous public health benefits. The underlying pathology of AD precedes the onset of cognitive

NIH ENIGMA Center grant U54EB020403, which is supported by the Big Data to Knowledge (BD2K) Centers of Excellence program. Data collection and sharing for this project was funded by the Alzheimer's Disease Neuroimaging Initiative (ADNI) (National Institutes of Health Grant U01 AG024904) and DOD ADNI (Department of Defense award number W81XWH-12-2-0012). The funders had no role in study design, data collection and analysis, decision to publish, or preparation of the manuscript.

Competing Interests: The authors have declared that no competing interests exist.

symptoms by many years, and efforts are underway to find reliable preclinical diagnostic biomarkers. The discovery of APOE as the most prevalent known genetic risk factor for AD [3, 4] has made it possible to study large numbers of genetically at-risk individuals before the onset of symptomatic memory impairment. This led to the concept of *preclinical AD* [5], which has now been validated in autopsy studies of non-demented elderly subjects with neuropathological evidence of AD [6–10], brain imaging studies [11–19], amyloid detection [20], and neuropsychological studies [21, 22]. Surface-based subregional structure analysis may offer additional benefits [17, 23–26], such as better visualization and increased statistical power, especially when detecting subtle genetic effects. As the paradigm in experimental therapeutics shifts toward earlier intervention and prevention, enrichment of treatment cohorts with APOE e4 carriers may improve diagnostic accuracy and may make it faster to evaluate treatments for preclinical AD [27, 28].

Structural magnetic resonance imaging (MRI) measurements of regional and whole brain tissue shrinkage, together with fluorodeoxyglucose positron emission tomography (FDG PET) measures of decline in the regional cerebral metabolic rate for glucose (CMRgl), and PET measurements of fibrillar amyloid-β (Aβ) burden are among the best established imaging biomarkers for preclinical detection and tracking of AD [29]. In AD research, commonly-used structural MRI measures include whole-brain [30–32], entorhinal cortex [33], hippocampus [25, 34–38], and temporal lobe volumes [39], as well as ventricular enlargement [35, 38, 40, 41]. Reductions in hippocampal and entorhinal cortex volumes become apparent in the early stages of memory decline and may anticipate progression to MCI and AD [42, 43]. Hippocampal atrophy measures from structural MRI are widely used, but do not generally detect more subtle alterations in hippocampal morphometry that may provide even more sensitive detection of early change.

In our recent work [25], we automatically segmented and constructed hippocampal surfaces from the baseline MR images of 725 subjects with known APOE genotype—including 167 with sporadic AD, 354 with MCI, and 204 normal controls. We also built high-order correspondences between hippocampal surfaces and computed multivariate statistics consisting of multivariate tensor-based morphometry (mTBM) and radial distance. Using Hotelling's T^2 test, we found significant morphological deformation in APOE e4 carriers relative to non-carriers in the entire cohort as well as in the non-demented (pooled MCI and control) subjects, affecting the left hippocampus more than the right (left hippocampus has a greater dose effect of APOE e4 than the right), and this effect was more pronounced in e4 homozygotes than heterozygotes. We now extend our work to a large, longitudinal dataset of brain MR images (N = 1925) from the Alzheimer's Disease Neuroimaging Initiative (ADNI) acquired at baseline, 6-month (N = 724), 12-month (N = 673) and 24-month (N = 533) intervals. We applied a novel surface mTBM system [40, 44–47] to create 3D maps of hippocampal atrophy associated with the APOE4 genotype. We hypothesized that (1) we would observe similar patterns of hippocampal deformation at each time points, as previously observed in the baseline study [25], and (2) the severity of hippocampal deformation and rate of decline would parallel APOE e4 gene dose.

Subjects and Methods

Subjects

Data used in this paper were obtained from the Alzheimer's Disease Neuroimaging Initiative (ADNI) database (adni.loni.usc.edu). The ADNI was launched in 2003 by the National Institute on Aging (NIA), the National Institute of Biomedical Imaging and Bioengineering (NIBIB), the Food and Drug Administration (FDA), private pharmaceutical companies and non-profit organizations, as a $60 million, 5-year public-private partnership. The primary goal

of ADNI has been to test whether serial magnetic reasonance imaging (MRI), positron emission tomography (PET), other biological markers, and clinical and neuropsychological assessment can be combined to measure the progression of mild cognitive impairment (MCI) and early Alzheimer's disease (AD). Determination of sensitive and specific markers of very early AD progression is intended to aid researchers and clinicians to develop new treatments and monitor their effectiveness, as well as lessen the time and cost of clinical trials.

The Principal Investigator of this initiative is Michael W. Weiner, MD, VA Medical Center and University of California—San Francisco. ADNI is the result of efforts of many co-investigators from a broad range of academic institutions and private corporations, and subjects have been recruited from over 50 sites across the U.S. and Canada. The initial goal of ADNI was to recruit 800 subjects but ADNI has been followed by ADNI-GO and ADNI-2. To date these three protocols have recruited over 1500 adults, ages 55 to 90, to participate in the research, consisting of cognitively normal older individuals, people with early or late MCI, and people with early AD. The follow up duration of each group is specified in the protocols for ADNI-1, ADNI-2 and ADNIGO. Subjects originally recruited for ADNI-1 and ADNI-GO had the option to be followed in ADNI-2. For up-to-date information, see www.adni-info.org.

At the time of downloading (September 2011), the baseline dataset consisted of 843 adults, including 233 elderly healthy controls (CTL), 410 subjects with mild cognitive impairment (MCI) and 200 AD patients. The 6-month follow up cohort consisted of 738 adults, including 214 elderly healthy controls (CTL), 359 subjects with mild cognitive impairment (MCI) and 165 AD patients. The 12-month follow up cohort consisted of 685 adults, including 203 elderly healthy controls (CTL), 338 subjects with mild cognitive impairment (MCI) and 144 AD patients. The 24-month follow up cohort consisted of 543 adults, including 178 elderly healthy controls (CTL), 254 subjects with mild cognitive impairment (MCI) and 111 AD patients. All subjects underwent thorough clinical and cognitive assessment at the time of acquisition, including the Mini-Mental State Examination [48], Clinical Dementia Rating (CDR) [49], and Delayed Logical Memory Test [50]. APOE genotyping was performed on DNA samples obtained from subjects' blood, using an APOE genotyping kit, as described in http://www.adni-info.org/Scientists/Pdfs/adniproceduresmanual12.pdf (also see http://www.adni-info.org for detailed information on blood sample collection, DNA preparation, and genotyping methods).

Participants were scanned with a standardized MRI protocol developed for this cohort [51]. We applied our hippocampal morphometry pipeline [25, 46] to reconstruct hippocampal meshes (detailed in Sec. 2.3). As a quality control, we manually checked all the constructed meshes. Similar to our prior work [25, 46], the exclusion criteria include: (1) failing the FIRST segmentation step probably due to the original images' resolution or contrast issue; (2) wrong surface topologies, such as the generated hippocampal surfaces have handles. In 6-month data, we manually excluded 3 subjects from CTL group, 6 subjects from MCI group and 5 subjects from AD group with wrong surface topologies. Similarly, in 12-month data, we manually excluded 3 subjects from CTL group, 8 subjects from MCI group, and 1 subject from AD group. In 24-month data, we manually excluded 2 subjects from CTL group, 5 subjects from MCI group, and 3 subjects from AD group. As a result, a total of 1925 ADNI longitudinal brain MR scans, including 211 controls (with a mean age of 76.41), 353 MCI (mean age: 75.06), and 160 AD (mean age: 74.88) from the 6-month follow-up cohort, 200 controls (mean age: 76.38), 330 MCI (mean age: 74.82), and 143 AD (mean age: 75.63) from the 12-month follow-up cohort, 176 controls (mean age: 76.44), 249 MCI (mean age: 74.75), and 108 AD (mean age: 75.17) from the 24-month follow-up cohort, were analyzed in the study. Table 1 gives detailed demographic data information on the subjects.

In our study, following prior work [23, 25, 46, 52], at each time point we pooled both the subjects who are heterozygotes APOE e4 carriers (e3/e4) and homozygotes APOE e4 carriers

Table 1. Table of Demographic Data by Diagnositic and Genotype Groups. Demographic data by diagnositic and genotype groups. N_6, N_{12}, and N_{24} indicate sample size of the 6-month, 12-month and 24-month follow up cohorts, respectively. The number of women in the samples is indicated in parentheses. Means are followed by standard deviations in parentheses for age and MMSE measures.

APOE genotype	CTL	MCI	AD	Total
0 APOE e4 allele (e3/e3)				
N_6	115(52)	127(44)	43(21)	285(117)
N_{12}	104(46)	120(41)	40(18)	264(105)
N_{24}	98(46)	90(33)	28(13)	216(92)
Age	76.51(±4.91)	76.13(±7.53)	76.82(±8.55)	76.39(±6.75)
MMSE	29.10(±1.13)	26.54(±3.36)	20.79(±5.00)	26.77(±4.06)
1 APOE e4 allele (e3/e4)				
N_6	43(21)	125(44)	61(25)	229(90)
N_{12}	44(21)	117(41)	58(25)	219(87)
N_{24}	40(19)	86(26)	45(18)	171(63)
Age	76.43(±4.42)	74.67(±6.65)	75.70(±6.06)	75.30(±6.13)
MMSE	28.79(±2.92)	25.41(±3.59)	21.25(±4.66)	24.96(±4.69)
2 APOE e4 alleles (e4/e4)				
N_6	3(1)	41(18)	32(13)	76(32)
N_{12}	4(2)	39(16)	28(10)	71(28)
N_{24}	4(2)	31(12)	21(9)	56(23)
Age	73.36(±2.92)	71.82(±5.74)	72.07(±6.91)	72.00(±6.13)
MMSE	29.09(±1.58)	25.68(±3.31)	20.72(±5.23)	23.88(±4.92)
Total				
N_6	161(74)	293(106)	136(59)	590(239)
N_{12}	152(69)	276(98)	126(53)	554(220)
N_{24}	142(67)	207(71)	94(40)	443(178)
Age	76.41(±4.76)	74.89(±7.07)	75.22(±7.31)	75.40(±6.58)
MMSE	29.01(±1.82)	25.94(±3.49)	20.99(±4.89)	25.71(±4.52)

doi:10.1371/journal.pone.0152901.t001

(e4/e4) together to form the *APOE e4 carriers group* and correlated presence of the APOE e4 allele with hippocampal morphometry, both (1) in the entire sample and (2) in non-demented (pooled MCI and controls) subjects. Throughout the paper, we call these two populations as the *full ADNI cohort* and *non-demented cohort*, respectively.

Processing Pipeline

Fig 1 summarizes the overall processing sequence. The original input data were the three-dimensional (3D) T1-weighted images from ADNI dataset (6-months, 12-months and 24-months), an example image is shown in Fig 1(a). First, we used the FIRST (FMRIB's Integrated Registration and Segmentation Tool) software [53] to segment the original data and obtain the hippocampus substructure. The hippocampal surfaces were automatically reconstructed based on binary segmentation results [25, 46]. Second, we generated a conformal grid for each surface with the holomorphic 1-form basis [54]. With the help of conformal grid, we can compute the conformal representation as the "feature image" of a surface. Third, we registered the feature image of each surface in the dataset to a common template with an inverse consistent surface fluid registration algorithm. Finally, we studied the longitudinal differences between different groups with the mTBM statistics [44] together with the radial distance. The similar processing pipeline was used in several of our prior works [25, 40, 47, 55–57].

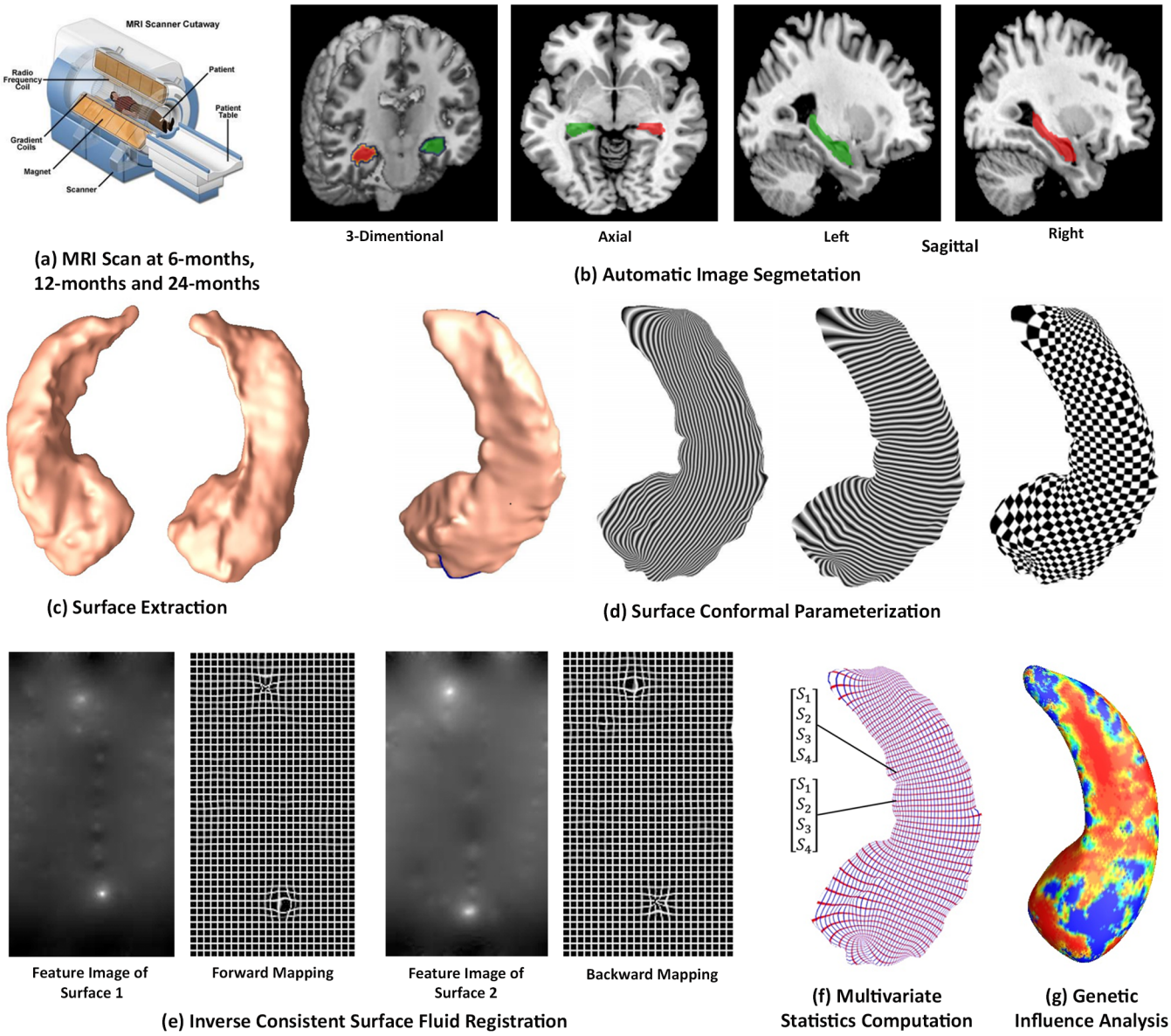

Fig 1. Overall Processing Sequence. (a): Longitudinal data (6-months, 12-months and 24-months) were obtained from the Alzheimer's Disease Neuroimaging Initiative (ADNI) database; (b) automatic hippocampus segmentation with FIRST software [53]; (c) hippocamal surface reconstruction with marching cube method [58]; (d) hippocampal surface conformal parameterization with holomorphic 1-forms [54]; (e) inverse consistent surface fluid registration of hippocampal surfaces [46]; (f) multivariate statistics [44] consisting of mTBM and radial distance; (g) longitudinal genetic influence of APOE e4 allele on hippocampal morphometry.

doi:10.1371/journal.pone.0152901.g001

Hippocampus Segmentation and Surface Modeling

In the process of segmentation, we used FIRST [53] to automatically process all T1-weighted MR images. FIRST is a model based subcortical structure segmentation and registration tool developed as part of the FSL library, which is written mainly by members of the Analysis Group, FMRIB, Oxford, UK. Within FIRST, we ran the *run_first_all* routine with default parameters tuned by FIRST as optimal for hippocampal segmentation. For now, we took three-phase image which contains the labels of the left and right hippocampi. The binary image of each side of hippocampus was obtained by a simple thresholding process. Fig 1(b) shows an

example of segmented hippocampus substructure. Then hippocampal surfaces were constructed with the marching cubes algorithm [58]. After mesh refinement [25, 46], we obtained smooth surfaces that are suitable for generating conformal grids. Finally, with the help of global affine transformation with a nine-parameter (three parameters for translation, three parameters for rotation, and three parameters for scaling) matrix that was computed by FIRST, the smoothed meshes were aligned into the MNI standard space. Fig 1(c) shows a pair of reconstructed hippocampal surfaces.

Conformal Grid Generation and Surface Conformal Representation

To facilitate hippocampal shape analysis, we generated a conformal grid on each surface, which is used as a canonical space for surface registration. On each hippocampal surface, we computed its conformal grid with holomorphic 1-form basis [44, 54]. Fig 1(d) shows an example hippocampal surface with its exact 1-form basis, conjugate 1-form basis and holomorphic 1-form basis [44, 54]. In the picture, the overlaid texture is used to demonstrate the computed 1-form bases. The checkboard texture is used to show the angle preserving property.

We adopted surface conformal representation [25, 46] to obtain surface geometric features for automated surface registration. It consists of the conformal factor and mean curvature, encoding both intrinsic surface structure and information on its 3D embedding. After we computed these two local features on each surface point, we computed their summation and then linearly scaled the dynamic range of the summation into [0, 255] to obtain a feature image for the surface.

Hippocampal Surface Registration with Inverse-Consistent Surface Fluid Registration

For longitudinal morphometric analysis, we need to register each individual hippocampal surface to a common template surface. With surface conformal parameterization and conformal representation, we generalized the well-studied image fluid registration algorithm [59, 60] to general surfaces. Furthermore, most image registration algorithms in the literature are not symmetric, i.e., the correspondences established between the two images depend on which image is assigned as the deforming image and which is the non-deforming target image. An asymmetric algorithm can be problematic as it tends to penalize the expansion of image regions more than shrinkage [61]. Thus, in our system, we further extended the surface fluid registration method to an inverse-consistent framework [62]. The obtained surface registration is diffeomorphic. For details of our inverse-consistent surface fluid registration method, we refer to [46]. Fig 1(e) illustrates the surface inverse consistent fluid registration method.

Surface Multivariate Morphometry Statistics

Our multivariate morphometry statistical analysis consists of mTBM [25, 40, 44, 46] and radial distance analysis [35, 63]. This combines complementary information from mTBM, which measures deformation within surfaces, and radial distance, which measures hippocampal size in terms of the surface normal direction.

As in our prior work [44], the mTBM was computed as a 3×1 vector consisting of the "Log-Euclidean metric" [64], computed as the matrix logarithm of the deformation tensor. mTBM statistics have been carefully studied in brain structure morphology analyses and they can detect signals more powerfully than more standard Jacobian matrix statistics [40, 45–47, 55]. Given the hippocampal tube-like shape, its atrophy and enlargement directly affect the distance from each surface point to its medial core (analogous to the center line in a tube). We call this distance the *radial distance* of a hippocampal surface. We formed the new multivariate surface morphometry statistic as a 4×1 vector consisting of the mTBM and radial distance (Fig 1(f)).

Statistical Group Difference

To assess group differences with multivariate statistics, we applied Hotelling's T^2 test [65–68] on sets of values of the new multivariate statistics. For each surface vertex, given two groups of n×4-dimensional vectors, S_i, i = 1,2,. . ., p,T_j, j = 1,2,. . ., q, we used the Mahalanobis distance M to measure the group mean difference,

$$M = \frac{N_S N_T}{N_S + N_T}(\bar{S} - \bar{T})^T \Sigma^{-1}(\bar{S} - \bar{T}).$$

where N_s and N_T are the numbers of subjects in the two groups, $\bar{S}$ and $\bar{T}$ are the means of the two groups and Σ is the combined covariance matrix of the two groups [40, 44, 69].

Next, for each hippocampal surface point, we ran a permutation test with 10,000 random assignments of subjects to different groups to estimate the statistical significance of the areas with group difference in surface morphometry. We also used a pre-defined statistical threshold of $p = 0.05$ at each surface point to estimate the overall significance of the group difference maps by non-parametric permutation testing [70, 71]. In each case, the covariate (group membership) was permuted 10,000 times and a null distribution was developed for the area of the average surface with group difference statistics above the pre-defined threshold in the significance map. The *overall significance of the map* is defined as the probability of finding, by chance alone, a statistical map with at least as large a surface area beating the pre-defined statistical threshold of $p = 0.05$. The permutation test on the overall rejection areas is used to evaluate the significance of overall experimental results and correct the overall significant p-values for multiple comparisons. Fig 1(g) shows an example of the significance p-map with uncorrected p-values, which is used to visualize the surface regions with significant differences between groups.

Results

Similar to our prior work [25], we mainly focused on studying the effects of APOE e4 genotype on hippocampal morphometry in two populations, (1) the full ADNI cohort; and (2) the non-demented cohort, i.e., people with MCI and normal control subjects. APOE e3 is the most prevalent allelic variant and considered the human wild type. In a gene-dose dependent pattern, APOE e4 increases and APOE e2 decreases susceptibility to "sporadic" and late onset AD [3, 4, 72–75]. APOE e4 is the focus of research in this paper. We took an approach similar to our prior work [23, 25], and excluded e2 carriers (with the result that a total of 60 e2 allele carriers were excluded from the study).

Results in the Full ADNI Cohorts for Three Follow Up Intervals

To explore whether the presence of the APOE e4 allele was associated with greater hippocampal atrophy, we studied the effects of APOE e4 genotype in three follow up full ADNI cohorts. Fig 2 shows the statistical p-maps for comparisons between e4 carriers (e3/e4 and e4/e4) and e4 non-carriers (e3/e3) in these three different follow up intervals, specifically, (a) for 6-month follow up (N = 590, 285 non-carriers vs. 305 carriers), (b) for 12-month (N = 555, 265 non-carriers vs. 290 carriers), and (c) for 24-month (N = 444, 218 non-carriers vs. 226 carriers). Non-blue colours show vertices with statistical differences at the nominal 0.05 level, uncorrected for multiple comparisons. After correcting for multiple comparisons, the differences remained highly significant ($p<0.0001$ for 6-months and 12-months, $p<0.0005$ for 24-months).

To explore whether APOE e4 allele dose affects hippocampal surface morphometry and how this atrophy is related to normal aging, we studied hippocampal morphometry differences between persons homozygous for the APOE e4 allele and those heterozygous in three follow

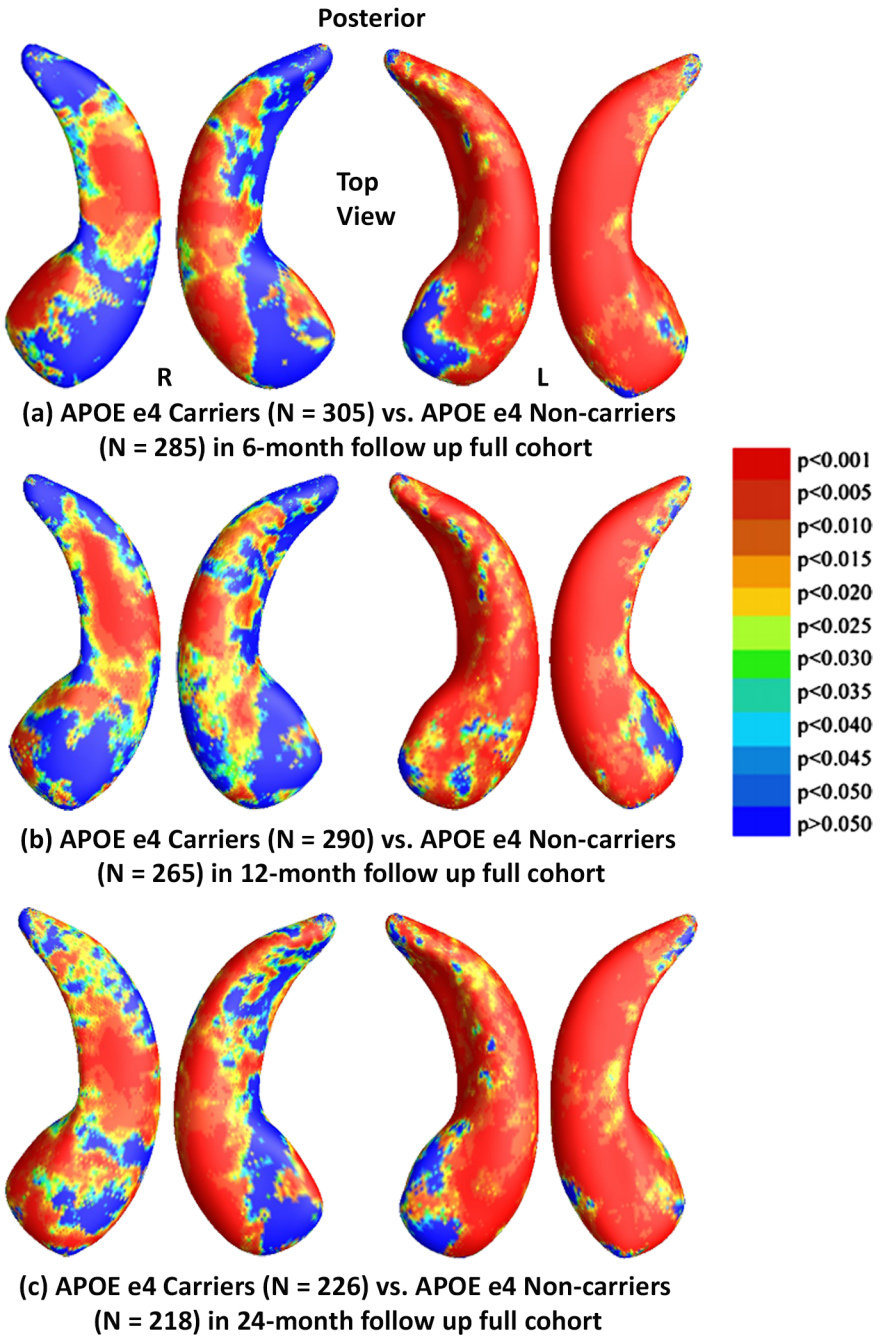

Fig 2. Shape Differences between Non-carriers and Carriers in Full ADNI. (a), (b) and (c): Illustration of local shape differences (*p*-values) between the APOE e4 carriers **(e3/e4 and e4/e4)** and non-carriers **(e3/e3)** in the full ADNI cohorts at 6-months, 12-months and 24-months respectively. Non-blue colours show vertices with statistical differences, at the nominal 0.05 level, uncorrected. The overall significance after multiple comparisons with permutation test is: (a) $p < 0.0001$, (b) $p < 0.0001$, (c) $p < 0.0005$.

doi:10.1371/journal.pone.0152901.g002

up cohorts. Fig 3 shows the statistical *p*-maps for these three different follow up time intervals, specifically, (a) for 6-month follow up (N = 305, 76 e4 homozygotes vs. 229 e4 heterozygots), (b) for 12-month (N = 290, 71 e4 homozygotes vs. 219 heterozygots), and (c) for 24-month (N = 226, 56 e4 homozygotes vs. 170 heterozygots). After correcting for multiple comparisons,

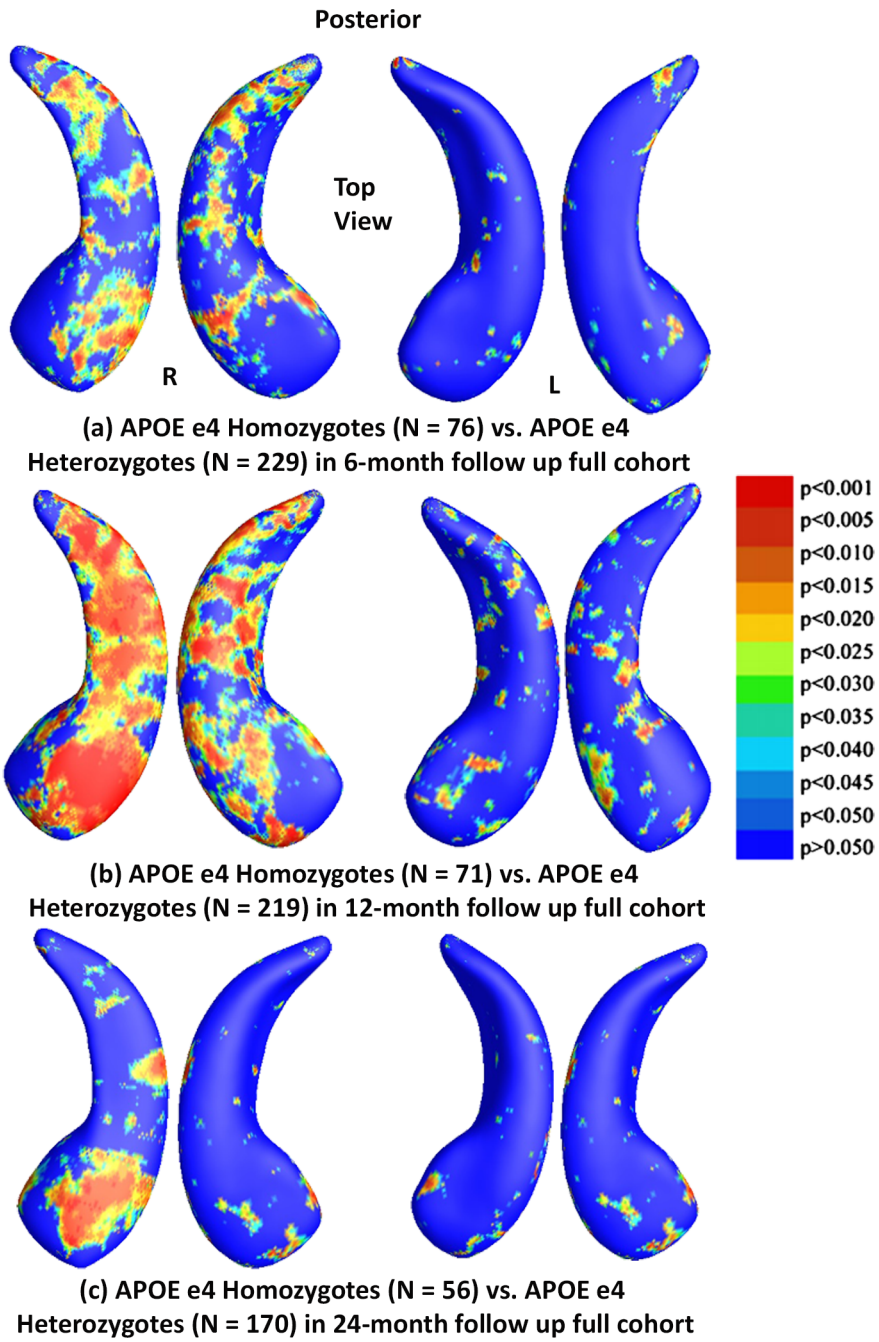

Fig 3. Shape Differences between Heterozygotes and Homozygotes in Full ADNI. (a), (b) and (c): Illustration of local shape differences (*p*-values) between the APOE e4 homozygotes (e4/e4) and heterozygotes (e3/e4) in the full ADNI cohorts at 6-months, 12-months and 24 months, respectively. Non-blue colours show vertices with statistical differences, at the nominal 0.05 level, uncorrected. The overall significance after multiple comparisons with permutation test is: (a) $p < 0.0117$, (b) $p < 0.0024$, (c) $p < 0.0959$.

doi:10.1371/journal.pone.0152901.g003

the differences remained significant for the 6- and 12-month but not for the 24-month follow up cohort ($p<0.0117$ for 6-months, $p<0.0024$ for 12-months, $p<0.0959$ for 24-months).

We also studied hippocampal morphometry differences between APOE e4 non-carriers and carriers with different e4 dose. Figs 4 and 5 show how APOE e4 non-carriers differ in

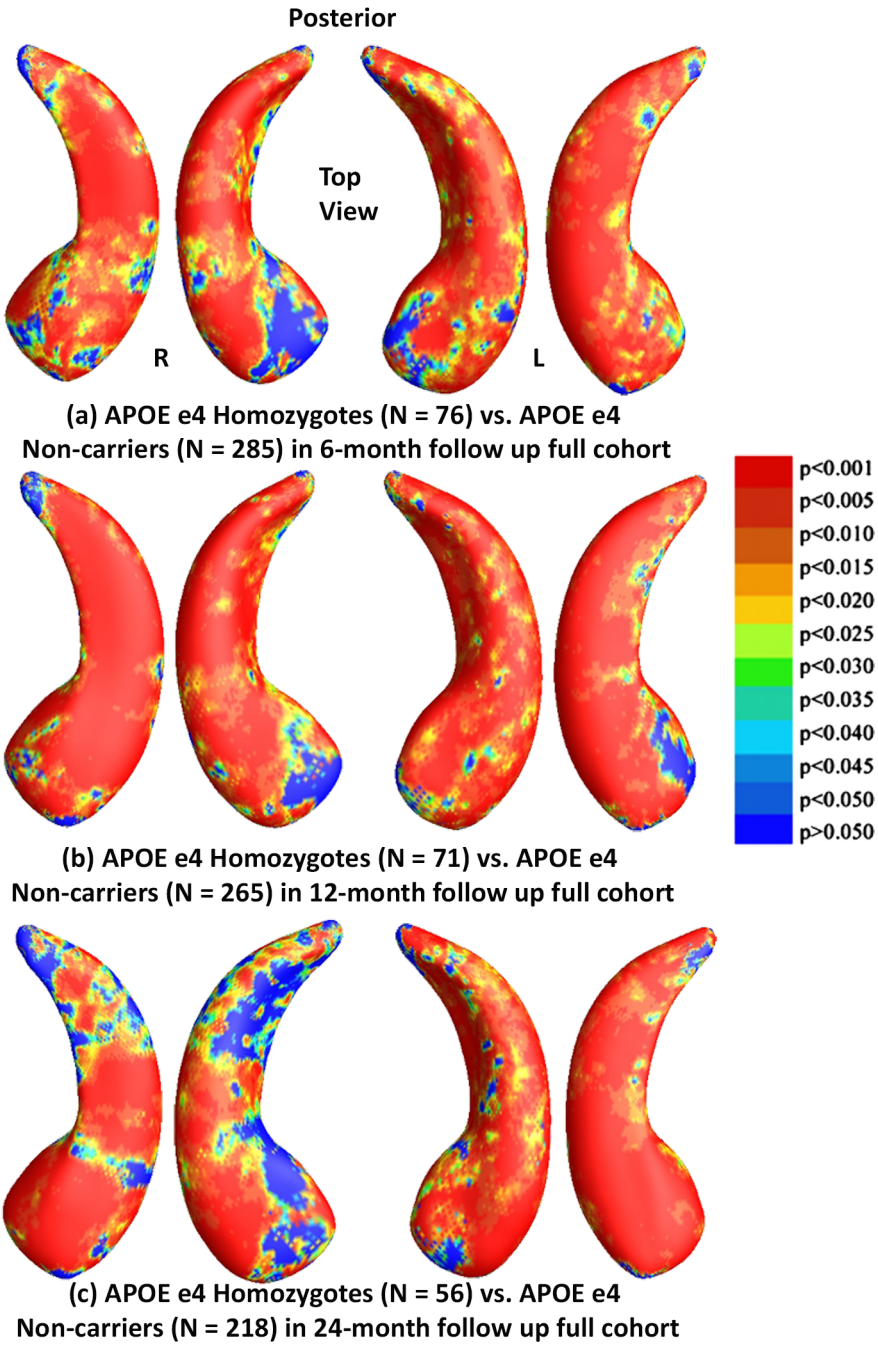

Fig 4. Shape Differences between Non-carriers and Homozygotes in Full ADNI. (a), (b) and (c): Illustration of local shape differences (*p*-values) between the APOE e4 homozygotes (e4/e4) and non-carriers (e3/e3) in the full ADNI cohorts at 6-months, 12-months and 24 months, respectively. Non-blue colours show vertices with statistical differences, at the nominal 0.05 level, uncorrected. The overall significance after multiple comparisons with permutation test is: (a) $p < 0.0001$, (b) $p < 0.0001$, (c) $p < 0.0001$.

doi:10.1371/journal.pone.0152901.g004

hippocampal shape from e4 homozygotes and heterozygotes, respectively. Fig 4 shows the statistical *p*-maps for comparisons between e4 homozygotes and non-carriers for (a) 6-month follow up (N = 361, 76 e4 homozygotes vs. 285 non-carriers), (b) for 12-month (N = 336, 71 e4 homozygotes vs. 265 non-carriers), and (c) for 24-month (N = 274, 56 e4

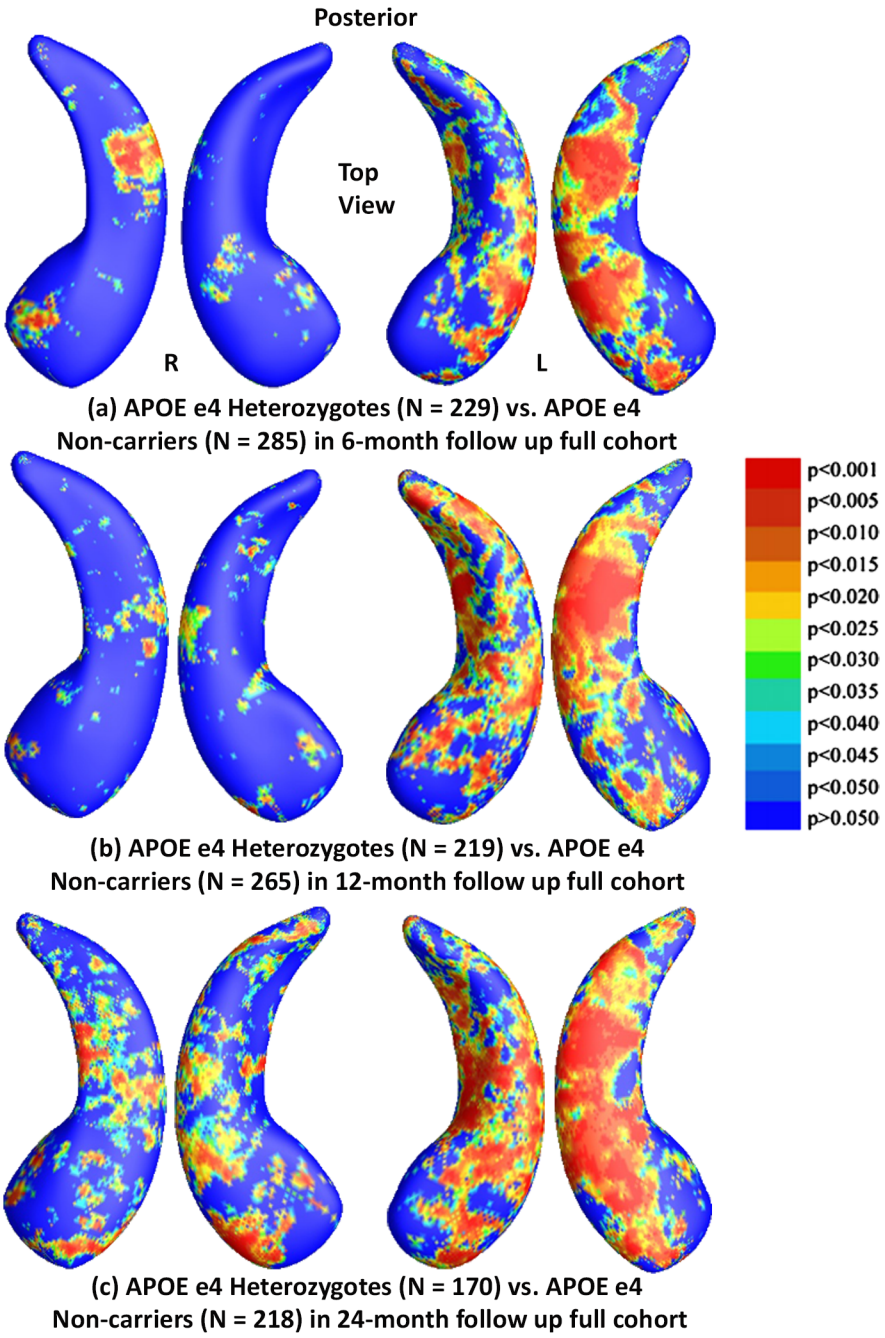

Fig 5. Shape Differences between Non-carriers and Heterozygotes in Full ADNI. (a), (b) and (c): Illustration of local shape differences (*p*-values) between the APOE e4 heterozygotes (e3/e4) and non-carriers (e3/e3) in the full ADNI cohorts at 6-months, 12-months and 24 months, respectively. Non-blue colours show vertices with statistical differences, at the nominal 0.05 level, uncorrected. The overall significance after multiple comparisons with permutation test is: (a) $p < 0.0116$, (b) $p < 0.0039$, (c) $p < 0.0003$.

doi:10.1371/journal.pone.0152901.g005

homozygotes vs. 170 non-carriers). After correcting for multiple comparisons, the differences remained significant for all three cohorts ($p<0.0001$ for all timepoints). Fig 5 shows the statistical *p*-maps for comparisons between e4 heterozygotes and non-carriers for (a) for 6-month follow up (N = 514, 229 e4 heterozygotes vs. 285 non-carriers), (b) for 12-month

(N = 484, 219 e4 heterozygotes vs. 265 non-carriers), and (c) for 24-month (N = 388, 170 e4 heterozygotes vs. 218 non-carriers). After correcting for multiple comparisons, the differences remained significant for all three cohorts ($p<0.0116$ for 6-months, $p<0.0039$ for 12-months, $p<0.0003$ for 24-months).

Results in the Non-demented ADNI Cohorts for Three Follow Up Intervals

We also conducted similar studies of APOE e4 genotype in three follow up non-demented ADNI cohorts. Fig 6 shows statistical *p*-maps for comparisons between e4 carriers and non-carriers in non-demented cohorts of three different follow up intervals, specifically, (a) for 6-month follow up (N = 454, 242 non-carriers vs. 212 e4 carriers), (b) for 12-month (N = 429, 225 non-carriers vs. 204 e4 carriers), and (c) for 24-month (N = 350, 190 non-carriers vs. 160 e4 carriers). Non-blue colours show vertices with statistical differences at the nominal 0.05 level, uncorrected for multiple comparisons. After correcting for multiple comparisons, the differences remained significant for all three cohorts ($p<0.0010$ for 6-months, $p<0.0005$ for 12-months, $p<0.0015$ for 24-months).

Similar to the full ADNI cohort studies, Fig 7 shows the statistical *p*-maps for comparisons between e4 homozygotes and heterozygotes in non-demented cohorts of three different follow up intervals, specifically, (a) for 6-month follow up (N = 212, 44 homozygotes vs. 168 heterozygotes), (b) for 12-month (N = 204, 43 homozygotes vs. 161 heterozygotes), and (c) for 24-month (N = 160, 35 homozygotes vs. 125 heterozygotes). After correcting for multiple comparisons, the differences only remained significant for 12-month follow up cohort ($p<0.0204$) and not for the other two cohorts ($p<0.1351$ for 6-months, $p<0.1870$ for 24-months).

We also studied hippocampal morphometry differnces between APOE e4 non-carriers and carriers with different e4 dose in the non-demented cohorts. Fig 8 shows the statistical *p*-maps for comparisons between e4 homozygotes and non-carriers in three different follow up intervals, specifically, (a) for 6-month follow up (N = 286, 44 homozygotes vs. 242 non-carriers), (b) for 12-month (N = 268, 43 homozygotes vs. 225 non-carriers), and (c) for 24-month (N = 225, 35 homozygotes vs. 190 non-carriers). After correcting for multiple comparisons, the differences remained significant for 6- and 12-month follow up cohorts ($p<0.0035$ for 6-months and $p<0.0010$ for 12-months) but not for 24-month cohorts ($p<0.0770$ for 24-months Fig 9). shows the statistical *p*-maps for comparisons between e4 heterozygotes and e4 non-carriers, specifically, (a) for 6-month follow up (N = 410, 168 heterozygotes vs. 242 non-carriers), (b) for 12-month (N = 386, 161 homozygotes vs. 225 non-carriers), and **(c)** for 24-month (N = 315, 125 heterozygotes vs. 190 non-carriers). After correcting for multiple comparisons, the differences remained significant for 6- and 24-month follow up cohorts ($p<0.0058$ for 6-months and $p<0.0110$ for 24-months) but not for 12-month follow up cohorts ($p<0.1191$ for 12-months).

Cumulative Distribution Functions of the *p*-values in the Statistical *p*-maps

In Fig 10, we created a set of cumulative distribution functions (CDF) of the *p*-values observed in four group difference experiments in the full ADNI cohort. We chose those experimental results that passed the permutation based multiple comparison tests (i.e., after correcting for multiple comparisons, $p<0.05$). Since there are too few homozygote samples in the 24-month follow up cohort (56 subjects in the full ADNI cohort), we also excluded the homozygote related CDFs from the 24-month follow up cohort. The CDFs of *p*-values are plotted against the corresponding *p*-value that would be expected, under the null hypothesis

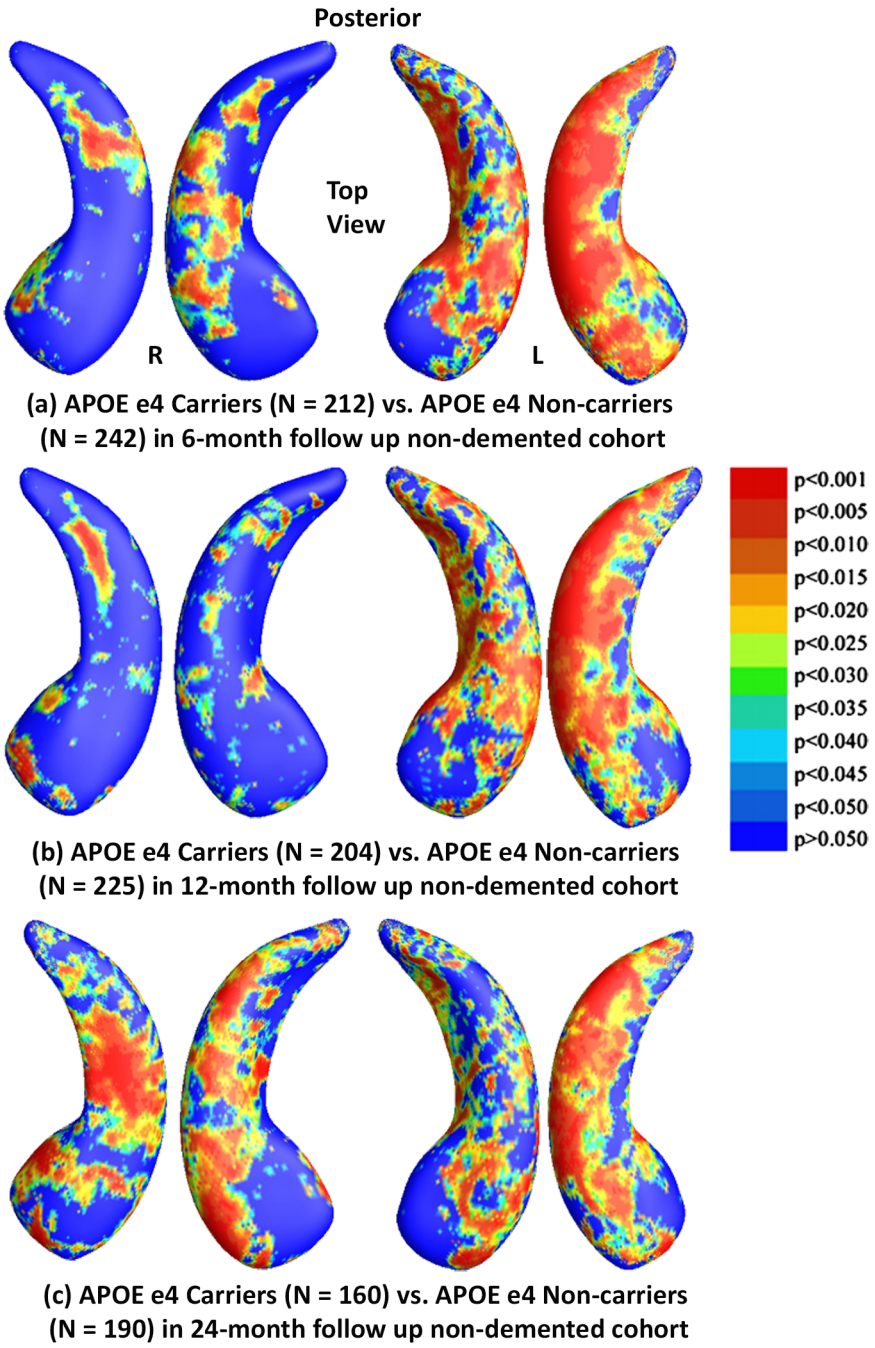

Fig 6. Shape Differences between Non-carriers and Carriers in Nondemented. (a), (b) and (c): Illustration of local shape differences (*p*-values) between the APOE e4 carriers **(e3/e4 and e4/e4)** and non-carriers **(e3/e3)** in the non-demented cohorts at 6-months, 12-months and 24-months, respectively. Non-blue colours show vertices with statistical differences, at the nominal 0.05 level, uncorrected. The overall significance after multiple comparisons with permutation test is: (a) $p < 0.001$, (b) $p < 0.0005$, (c) $p < 0.0015$.

doi:10.1371/journal.pone.0152901.g006

of no group difference, for all above experiments shown in Fig 10. For null distributions, the cumulative distribution of *p*-values is expected to fall approximately along the dotted line. Large deviations from that curve are associated with significant signal, and greater effect sizes represented by larger deviations. The theory of false discovery rates (FDR) [76] gives

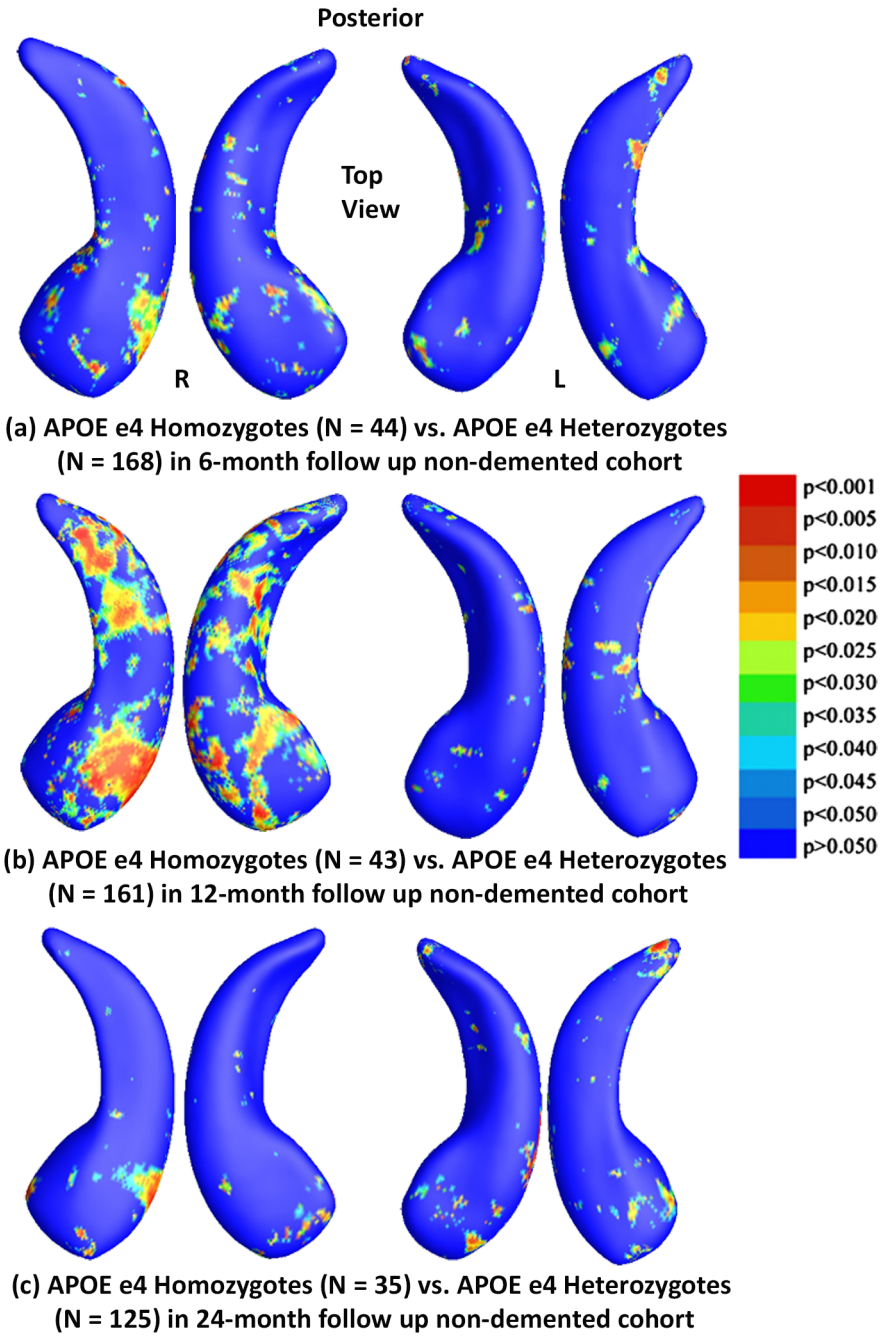

Fig 7. Shape Differences between Heterozygotes and Homozygotes in Nondemented. (a), (b) and (c): Illustration of local shape differences (*p*-values) between the APOE e4 homozygotes (e4/e4) and heterozygotes (e3/e4) in the non-demented cohorts at 6-months, 12-months and 24-months, respectively. Non-blue colours show vertices with statistical differences, at the nominal 0.05 level, uncorrected. The overall significance after multiple comparisons with permutation test is: (a) $p < 0.1351$, (b) $p < 0.0204$, (c) $p < 0.187$.

doi:10.1371/journal.pone.0152901.g007

formulae for thresholds that tend to control false positives at a known rate. This protocol was adopted in several of our prior papers [25, 40, 44, 46, 47, 55, 77] as an empirical standard to compare effects in group difference analysis. The deviation of the statistics from the null distribution generally increased longitudinally from 6-month, to 12-month and 24-month

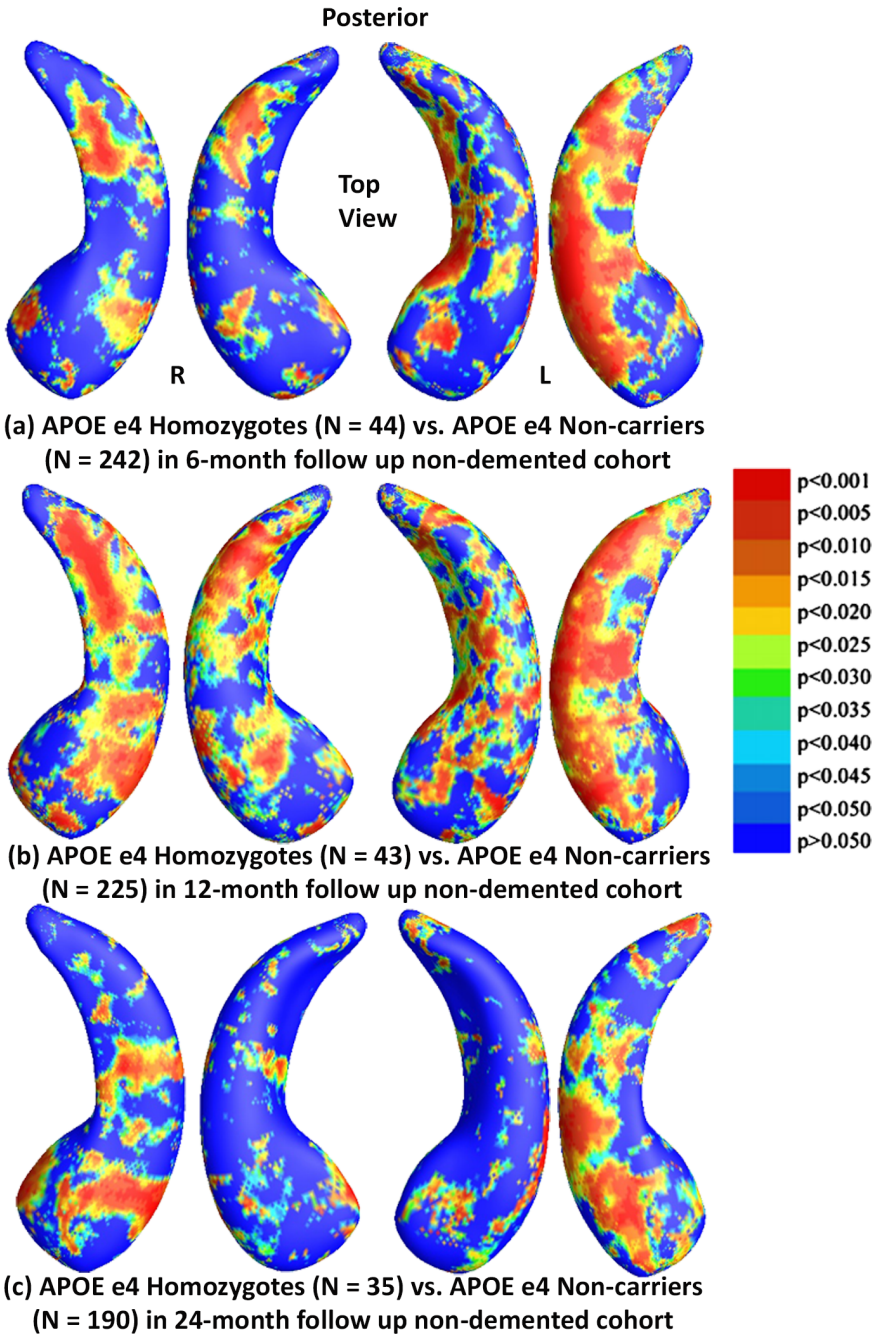

Fig 8. Shape Differences between Non-carriers and Homozygotes in Nondemented. (a), (b) and (c): Illustration of local shape differences (*p*-values) between the APOE e4 homozygotes **(e4/e4)** and non-carriers **(e3/e3)** in the non-demented cohorts at 6-months, 12-months and 24-months, respectively. Non-blue colours show vertices with statistical differences, at the nominal 0.05 level, uncorrected. The overall significance after multiple comparisons with permutation test is: (a) $p < 0.0035$, (b) $p < 0.001$, (c) $p < 0.077$.

doi:10.1371/journal.pone.0152901.g008

follow up data in the full ADNI cohort. It shows that the continually increasing differences in atrophy between APOE e4 carriers and non-carriers (Fig 10(a)), APOE e4 heterozygotes and homozygotes (Fig 10(b)), APOE e4 homozygotes and non-carriers (Fig 10(c)), and APOE e4 heterozygotes and non-carriers (Fig 10(d)).

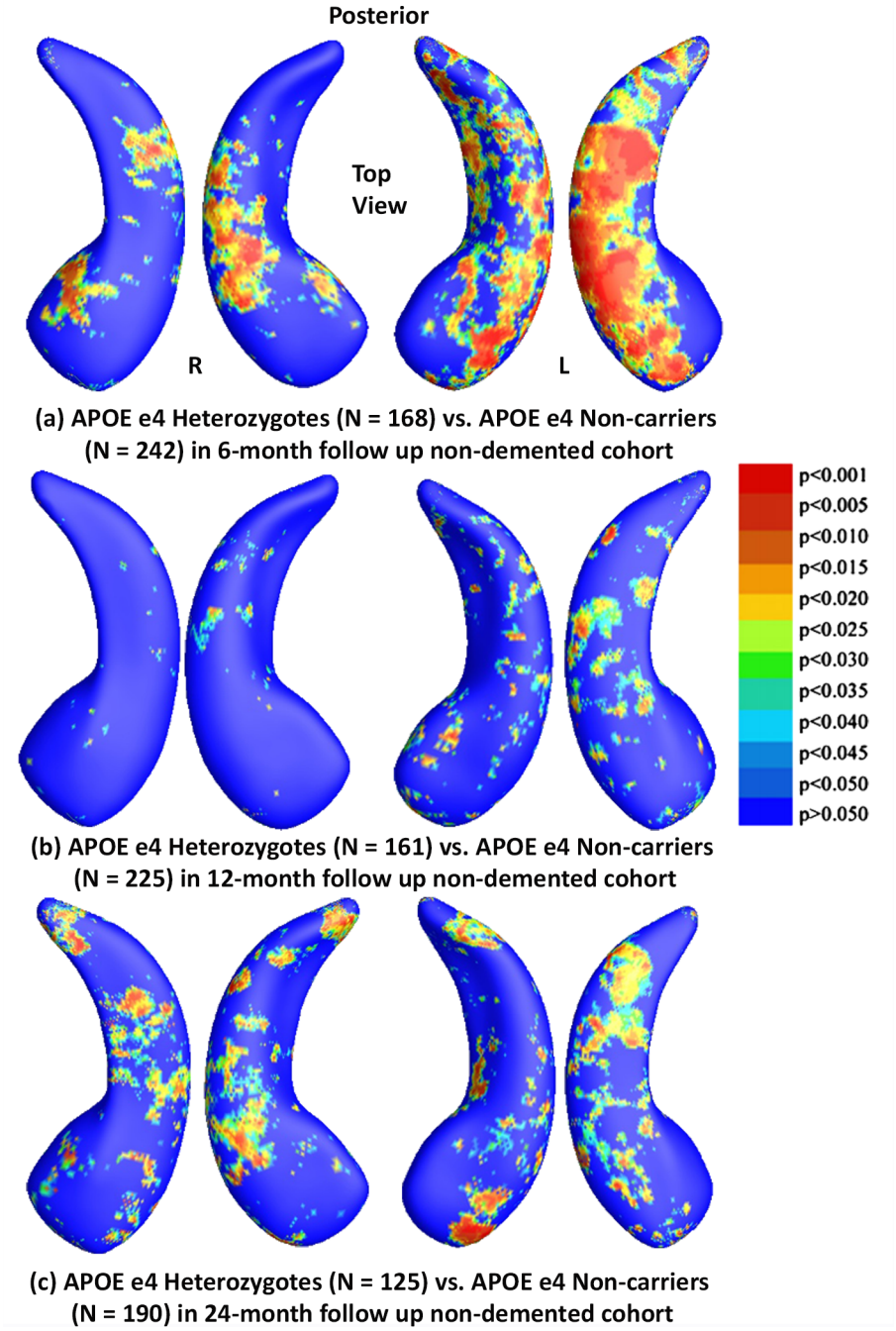

Fig 9. Shape Differences between Non-carriers and Heterozygotes in Nondemented. (a), (b) and (c): Illustration of local shape differences (*p*-values) between the APOE e4 heterozygotes **(e3/e4)** and non-carriers **(e3/e3)** in the non-demented cohorts at 6-months, 12-months and 24-months, respectively. Non-blue colours show vertices with statistical differences, at the nominal 0.05 level, uncorrected. The overall significance after multiple comparisons with permutation test is: (a) $p < 0.0058$, (b) $p < 0.1191$, (c) $p < 0.011$.

doi:10.1371/journal.pone.0152901.g009

Discussion

Our analyses of the full ADNI cohort revealed significant differences between APOE e4 carriers and non-carriers in all three follow up cohorts (Fig 2), between e4 homozygotes and

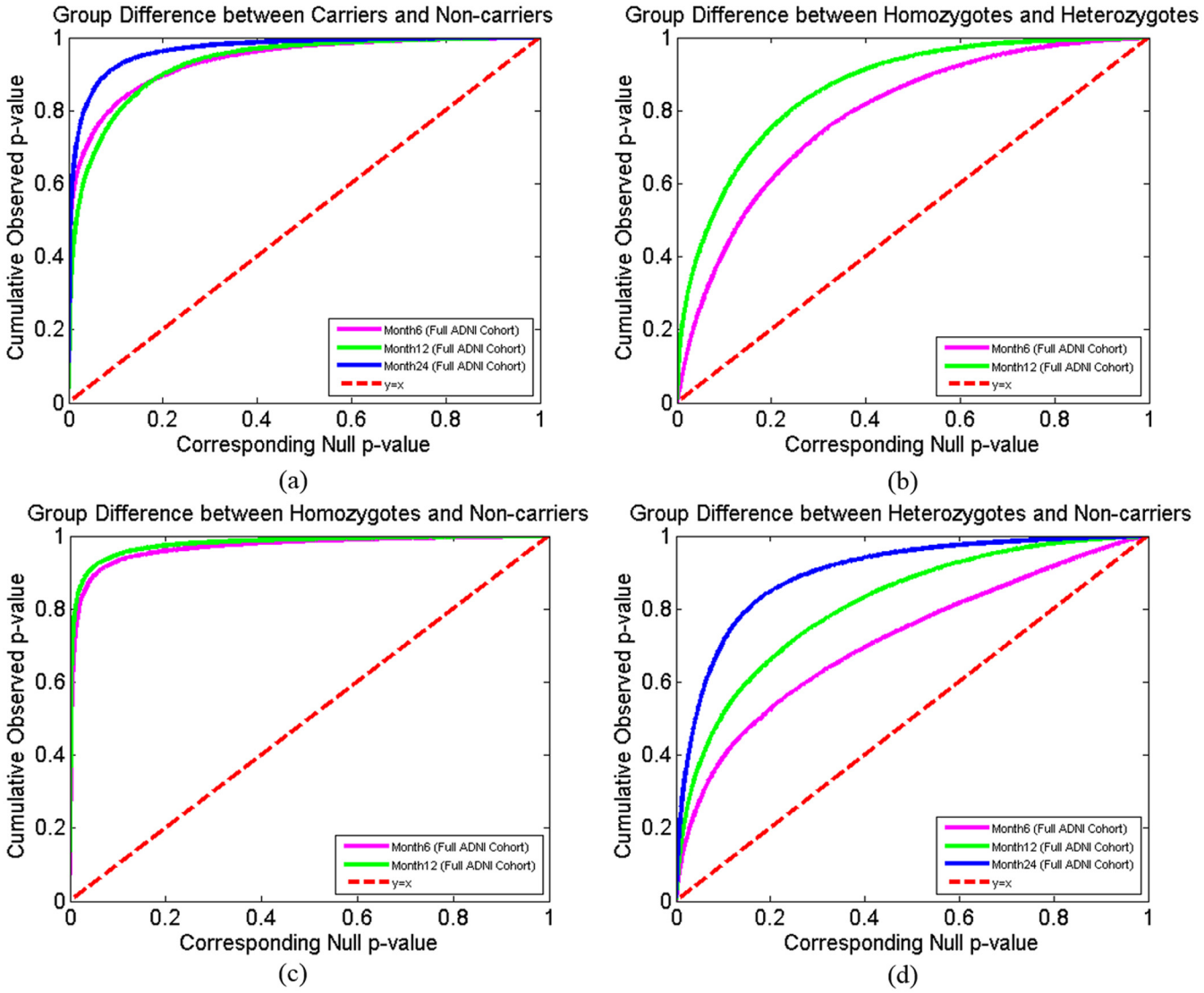

Fig 10. Cumulative Distribution Function Plots Comparison. Cumulative Distribution Function (CDF) plots comparison, between: (a). APOE e4 carriers **(e3/e4 and e4/e4)** and non-carriers **(e3/e3)**, (b). APOE e4 homozygotes **(e4/e4)** and heterozygotes **(e3/e4)**, (c). APOE e4 homozygotes **(e4/e4)** and non-carriers **(e3/e3)**, (d). APOE e4 heterozygotes **(e3/e4)** and non-carriers **(e3/e3)** in the full ADNI cohorts. The results demonstrate the accelarated hippocampal atrophy in the longitudinal study.

doi:10.1371/journal.pone.0152901.g010

heterozygotes in the 6- and 12-month follow up cohorts (Fig 3), between e4 homozygotes and non-carriers in all three follow up cohorts (Fig 4), and between e4 heterozygotes and non-carriers in all three follow up cohorts (Fig 5). Also, from the CDFs shown in Fig 10, there is a trend for group differences to generally become sharper over time. These results are consistent with our observations in the baseline cohort [25] and another prior work [78] in a relatively small dataset, showing a clear relationship between APOE genotype and hippocampal atrophy in the full ADNI cohort at all three follow up time intervals. In contrast, some investigators, e.g. [79–83], detected no APOE e4 gene dose effect on hippocampal atrophy. In the full ADNI cohort, a relatively large imaging cohort (N = 1925), we found that the APOE e4 dose was associated with greater hippocampal deformation (i.e., the CDF curves in Fig 10(c) are much steeper than those in Fig 10(d)). Although more rigorous statistical comparisons are necessary, from the *p*-

maps and CDF plots, we can observe the trend that in these groups shown in Fig 10(c) and 10 (d), APOE e4 homozygotes appear to differ more from non-carriers than do e4 heterozygotes. To our knowledge, this is the first study to apply a surface-based approach to evaluate longitudinal APOE e4 gene dose effects on hippocampal morphometry. Our findings confirm and extend our observation that APOE e4 gene dose correlates with the severity of hippocampal deformation, and support the use of MRI hippocampal morphometry as a valid imaging biomarker to track AD progression.

Findings in the non-demented subset were consistent with our previously reported baseline findings [25]. With few exceptions (homozygotes vs heterozygotes in 6- and 24-month follow up cohorts, heterozygotes and non-carriers in the 12-month follow up cohort and homozygotes and non-carriers in the 24-month follow up cohort), we found significant differences in APOE subgroups in all comparisons in each follow up cohort. However, the effects of e4 homozygosity on regional patterns of hippocampal morphometry at 24-months did not pass the permutation tests when compared to heterozygotes or non-carriers, probably reflecting insufficient statistical power, as sample sizes were much smaller (N = 35) than other subject numbers. In our prior work [25], we did not detect statistically significant differences between homozygotes and heterozygotes at baseline in the non-demented cohort, but we now find increasing differences between non-demented homozygotes and heterozygotes in the 12-month follow up cohort, as well as between homozygotes and non-carriers in both the 6- and 12-month follow up cohorts, supporting our hypothesis that there is an e4 gene dose effect for hippocampal deformation in the non-demented population.

Previous investigators [80, 84–86] reported greater atrophy of the right hippocampus when comparing e4 heterozygotes and homozygotes with non-carriers. In contrast, our results suggest e4 carriers in general, as well as heterozygous and homozygous subgroups have greater deformity of the left hippocampus compared to non-carriers. By contrast, differences between the e4 heterozygous and homozygous subgroups were greater on the right side than on the left. Our results are consistent with some prior work [23, 25, 78]. The reason for this laterality effect is unclear, but may suggest that the APOE e4 dose effects start from the left side and subsequently extend to the right.

There is an ever growing variety of methods for examining the structure and function of the hippocampus via *in vivo* MR images [87, 88]. Some examine the subfields of the hippocampal formation and subregions of the parahippocampal gyrus [89–94], which segment hippocampus into different regions and analyze the volume and shape changes in these subfields. These methods compute volumetric image registration between template and individual subjects and translate and visualize the deformation of surfaces. Surface-based hippocampal shape analyses rely primarily on two components. First, they build an appropriate representation and correspondence between hippocampal shapes. Second, they carry out group analysis within this common domain. Surface parameterization methods [54, 95, 96] create a canonical space to match hippocampal surfaces. When the canonical space is a sphere, approaches based on spherical harmonic functions (SPHARM) [97–99] use coefficients of the harmonic expansion to infer shape differences between patient groups and controls. Another group of methods aims to build dense correspondence between surfaces [40, 100, 101]. For example, the Large Deformation Diffeomorphic Metric Mapping (LDDMM) [102] has been used to deform labeled anatomical templates of the hippocampus onto new images, using a combination of manual landmarking of points on the hippocampus and 3D fluid image registration [100, 101, 103]. Other dense mapping methods register hippocampal surfaces with surface geometric features [24, 35, 46, 52, 104, 105]. For group difference analysis, some groups have used a single low dimensional feature vector [106–108], or other detailed local geometric features such as medial distance [35], the LDDMM metric [109], and tensor-based morphometry [40] for

detailed statistical shape analysis. This type of method benefits from high resolution information in the hippocampal surface representation and efficient numerical solutions to register and analyze surface deformations across subjects.

As noted in Shi, et al. [25], our current work has two main caveats. First, the ADNI participants are generally elderly, so they may not ideally represent patient populations in clinical prevention trials. Still, our current findings support the genetic influence of APOE genotype in non-demented cohorts. Second, we excluded APOE e2 carriers from our current study for a more focused study. We expect to conduct a thorough study on APOE e2 effects in our future research.

In conclusion, by applying our novel hippocampal morphometry system in the longitudinal ADNI datasets, we replicated the influence of APOE genotype on hippocampal morphometry observed at baseline [25], and demonstrated strong APOE e4 gene dose effects in the 6-month and 12-month follow up cohorts. In the future, we will continue developing novel imaging shape analysis systems to better detect genetic influences on the brain. We plan to apply this framework together with our ventricular morphometry system [40] and cortical thickness estimation system [77] in cognitively normal subjects to help detect preclinical AD [110, 111].

Acknowledgments

This work was funded by the National Institute on Aging (R21AG043760 to BL, JS, LCB, RJC and YW, R21AG049216 to JS, PMT and YW, R01AG031581 and P30AG19610 to RJC), the National Science Foundation (DMS-1413417, IIS-1421165 to YW), and the Arizona Alzheimer's Consortium (ADHS14-052688 to BL, JS and YW). BAG, PMT and YW are also supported, in part, by the NIH ENIGMA Center grant U54EB020403, which is supported by the Big Data to Knowledge (BD2K) Centers of Excellence program.

Data collection and sharing for this project was funded by the Alzheimer's Disease Neuroimaging Initiative (ADNI) (National Institutes of Health Grant U01 AG024904) and DOD ADNI (Department of Defense award number W81XWH-12-2-0012). ADNI-PI is Michael W. Weiner, MD(email: Michael.Weiner@ucsf.edu). A complete listing of ADNI investigators can be found at https://adni.loni.usc.edu/wp-content/uploads/how_to_apply/ADNI_Acknowledgement_List.pdf. Data used in preparation of this article were obtained from the ADNI (adni.loni.usc.edu). As such, the investigators within the ADNI contributed to the design and implementation of ADNI and/or provided data but did not participate in analysis or writing of this report. ADNI is funded by the National Institute on Aging, the National Institute of Biomedical Imaging and Bioengineering, and through generous contributions from the following: Alzheimer's Association; Alzheimer's Drug Discovery Foundation; Araclon Biotech; BioClinica, Inc.; Biogen Idec Inc.; Bristol-Myers Squibb Company; Eisai Inc.; Elan Pharmaceuticals, Inc.; Eli Lilly and Company; EuroImmun; F. Hoffmann-La Roche Ltd and its affiliated company Genentech, Inc.; Fujirebio; GE Healthcare;; IXICO Ltd.; Janssen Alzheimer Immunotherapy Research & Development, LLC.; Johnson & Johnson Pharmaceutical Research & Development LLC.; Medpace, Inc.; Merck & Co., Inc.; Meso Scale Diagnostics, LLC.; NeuroRx Research; Neurotrack Technologies; Novartis Pharmaceuticals Corporation; Pfizer Inc.; Piramal Imaging; Servier; Synarc Inc.; and Takeda Pharmaceutical Company. The Canadian Institutes of Rev December 5, 2013 Health Research is providing funds to support ADNI clinical sites in Canada. Private sector contributions are facilitated by the Foundation for the National Institutes of Health (www.fnih.org). The grantee organization is the Northern California Institute for Research and Education, and the study is coordinated by the Alzheimer's Disease Cooperative Study at the University of California, San Diego. ADNI data are disseminated by the Laboratory for Neuro Imaging at the University of Southern California.

Author Contributions

Conceived and designed the experiments: YW. Performed the experiments: BL JS YW. Analyzed the data: PMT RJC YW. Contributed reagents/materials/analysis tools: BAG LCB. Wrote the paper: BL PMT RJC YW.

References

1. Frey BJ. Alzheimer's disease.". 2003. Encyclopedia.com. 27 Mar. 2015 2003. Available from: http://www.encyclopedia.com/doc/1G2-3405700022.html.
2. Villemagne VL, Ataka S, Mizuno T, Brooks WS, Wada Y, Kondo M, et al. High striatal amyloid beta-peptide deposition across different autosomal Alzheimer disease mutation types. Arch Neurol. 2009; 66(12):1537–44. doi: 10.1001/archneurol.2009.285 PMID: 20008660.
3. Corder EH, Saunders AM, Strittmatter WJ, Schmechel DE, Gaskell PC, Small GW, et al. Gene dose of apolipoprotein E type 4 allele and the risk of Alzheimer's disease in late onset families. Science. 1993; 261(5123):921–3. Epub 1993/08/13. PMID: 8346443.
4. Saunders AM, Strittmatter WJ, Schmechel D, George-Hyslop PH, Pericak-Vance MA, Joo SH, et al. Association of apolipoprotein E allele epsilon 4 with late-onset familial and sporadic Alzheimer's disease. Neurology. 1993; 43(8):1467–72. PMID: 8350998.
5. Sperling RA, Aisen PS, Beckett LA, Bennett DA, Craft S, Fagan AM, et al. Toward defining the preclinical stages of Alzheimer's disease: recommendations from the National Institute on Aging-Alzheimer's Association workgroups on diagnostic guidelines for Alzheimer's disease. Alzheimers Dement. 2011; 7(3):280–92. Epub 2011/04/26. doi: 10.1016/j.jalz.2011.03.003 PMID: 21514248; PubMed Central PMCID: PMC3220946.
6. Dickson DW, Crystal HA, Mattiace LA, Masur DM, Blau AD, Davies P, et al. Identification of normal and pathological aging in prospectively studied nondemented elderly humans. Neurobiol Aging. 1992; 13(1):179–89. Epub 1992/01/01. PMID: 1311804.
7. Gouras GK, Relkin NR, Sweeney D, Munoz DG, Mackenzie IR, Gandy S. Increased apolipoprotein E epsilon 4 in epilepsy with senile plaques. Ann Neurol. 1997; 41(3):402–4. Epub 1997/03/01. doi: 10.1002/ana.410410317 PMID: 9066363.
8. Bennett DA, De Jager PL, Leurgans SE, Schneider JA. Neuropathologic intermediate phenotypes enhance association to Alzheimer susceptibility alleles. Neurology. 2009; 72(17):1495–503. Epub 2009/04/29. doi: 10.1212/WNL.0b013e3181a2e87d PMID: 19398704; PubMed Central PMCID: PMC2677477.
9. Kok E, Haikonen S, Luoto T, Huhtala H, Goebeler S, Haapasalo H, et al. Apolipoprotein E-dependent accumulation of Alzheimer disease-related lesions begins in middle age. Ann Neurol. 2009; 65(6):650–7. Epub 2009/06/27. doi: 10.1002/ana.21696 PMID: 19557866.
10. Caselli RJ, Walker D, Sue L, Sabbagh M, Beach T. Amyloid load in nondemented brains correlates with APOE e4. Neurosci Lett. 2010; 473(3):168–71. Epub 2010/02/16. doi: 10.1016/j.neulet.2010.02.016 PMID: 20153809; PubMed Central PMCID: PMC2851172.
11. Knickmeyer RC, Wang J, Zhu H, Geng X, Woolson S, Hamer RM, et al. Common variants in psychiatric risk genes predict brain structure at birth. Cereb Cortex. 2014; 24(5):1230–46. Epub 2013/01/04. doi: 10.1093/cercor/bhs401 PMID: 23283688; PubMed Central PMCID: PMC3977618.
12. Dean DC 3rd, Jerskey BA, Chen K, Protas H, Thiyyagura P, Roontiva A, et al. Brain differences in infants at differential genetic risk for late-onset Alzheimer disease: a cross-sectional imaging study. JAMA Neurol. 2014; 71(1):11–22. doi: 10.1001/jamaneurol.2013.4544 PMID: 24276092; PubMed Central PMCID: PMC4056558.
13. Reiman EM, Caselli RJ, Yun LS, Chen K, Bandy D, Minoshima S, et al. Preclinical evidence of Alzheimer's disease in persons homozygous for the epsilon 4 allele for apolipoprotein E. N Engl J Med. 1996; 334(12):752–8. Epub 1996/03/21. doi: 10.1056/NEJM199603213341202 PMID: 8592548.
14. Reiman EM, Chen K, Alexander GE, Caselli RJ, Bandy D, Osborne D, et al. Correlations between apolipoprotein E epsilon4 gene dose and brain-imaging measurements of regional hypometabolism. Proc Natl Acad Sci U S A. 2005; 102(23):8299–302. Epub 2005/06/04. 0500579102 [pii] doi: 10.1073/pnas.0500579102 PMID: 15932949; PubMed Central PMCID: PMC1149416.
15. Reiman EM, Chen K, Liu X, Bandy D, Yu M, Lee W, et al. Fibrillar amyloid-beta burden in cognitively normal people at 3 levels of genetic risk for Alzheimer's disease. Proc Natl Acad Sci U S A. 2009; 106(16):6820–5. Epub 2009/04/07. 0900345106 [pii] doi: 10.1073/pnas.0900345106 PMID: 19346482; PubMed Central PMCID: PMC2665196.

16. Morris JC, Roe CM, Xiong C, Fagan AM, Goate AM, Holtzman DM, et al. APOE predicts amyloid-beta but not tau Alzheimer pathology in cognitively normal aging. Ann Neurol. 2010; 67(1):122–31. Epub 2010/02/27. doi: 10.1002/ana.21843 PMID: 20186853; PubMed Central PMCID: PMC2830375.

17. Roussotte FF, Gutman BA, Madsen SK, Colby JB, Narr KL, Thompson PM, et al. Apolipoprotein E epsilon 4 allele is associated with ventricular expansion rate and surface morphology in dementia and normal aging. Neurobiol Aging. 2014; 35(6):1309–17. doi: 10.1016/j.neurobiolaging.2013.11.030 PMID: 24411483; PubMed Central PMCID: PMC3961511.

18. Filippini N, MacIntosh BJ, Hough MG, Goodwin GM, Frisoni GB, Smith SM, et al. Distinct patterns of brain activity in young carriers of the APOE-epsilon4 allele. Proc Natl Acad Sci U S A. 2009; 106 (17):7209–14. doi: 10.1073/pnas.0811879106 PMID: 19357304; PubMed Central PMCID: PMC2678478.

19. Erten-Lyons D, Dodge HH, Woltjer R, Silbert LC, Howieson DB, Kramer P, et al. Neuropathologic basis of age-associated brain atrophy. JAMA Neurol. 2013; 70(5):616–22. doi: 10.1001/jamaneurol.2013.1957 PMID: 23552688; PubMed Central PMCID: PMC3898525.

20. Baltes C, Princz-Kranz F, Rudin M, Mueggler T. Detecting amyloid-beta plaques in Alzheimer's disease. Methods Mol Biol. 2011; 711:511–33. doi: 10.1007/978-1-61737-992-5_26 PMID: 21279620.

21. Caselli RJ, Dueck AC, Osborne D, Sabbagh MN, Connor DJ, Ahern GL, et al. Longitudinal modeling of age-related memory decline and the APOE epsilon4 effect. N Engl J Med. 2009; 361(3):255–63. Epub 2009/07/17. doi: 10.1056/NEJMoa0809437 PMID: 19605830; PubMed Central PMCID: PMC2928998.

22. Caselli RJ, Dueck AC, Locke DE, Sabbagh MN, Ahern GL, Rapcsak SZ, et al. Cerebrovascular risk factors and preclinical memory decline in healthy APOE epsilon4 homozygotes. Neurology. 2011; 76 (12):1078–84. Epub 2011/02/18. doi: 10.1212/WNL.0b013e318211c3ae PMID: 21325652; PubMed Central PMCID: PMC3068011.

23. Morra JH, Tu Z, Apostolova LG, Green AE, Avedissian C, Madsen SK, et al. Automated mapping of hippocampal atrophy in 1-year repeat MRI data from 490 subjects with Alzheimer's disease, mild cognitive impairment, and elderly controls. NeuroImage. 2009; 45(1, Supplement 1):S3—S15. PMID: 19041724.

24. Qiu A, Taylor WD, Zhao Z, MacFall JR, Miller MI, Key CR, et al. APOE related hippocampal shape alteration in geriatric depression. NeuroImage. 2009; 44(3):620–6. Epub 2008/11/18. S1053-8119 (08)01121-X [pii] doi: 10.1016/j.neuroimage.2008.10.010 PMID: 19010425; PubMed Central PMCID: PMC2648826.

25. Shi J, Lepore N, Gutman BA, Thompson PM, Baxter LC, Caselli RJ, et al. Genetic influence of apolipoprotein E4 genotype on hippocampal morphometry: An N = 725 surface-based Alzheimer's disease neuroimaging initiative study. Hum Brain Mapp. 2014; 35(8):3903–18. Epub 2014/01/24. doi: 10.1002/hbm.22447 PMID: 24453132; PubMed Central PMCID: PMC4269525.

26. Roussotte FF, Gutman BA, Madsen SK, Colby JB, Thompson PM, Alzheimer's Disease Neuroimaging I. Combined effects of Alzheimer risk variants in the CLU and ApoE genes on ventricular expansion patterns in the elderly. J Neurosci. 2014; 34(19):6537–45. doi: 10.1523/JNEUROSCI.5236-13.2014 PMID: 24806679; PubMed Central PMCID: PMC4012312.

27. Caselli RJ, Reiman EM. Characterizing the preclinical stages of Alzheimer's disease and the prospect of presymptomatic intervention. J Alzheimers Dis. 2013; 33 Suppl 1:S405–16. doi: 10.3233/JAD-2012-129026 PMID: 22695623; PubMed Central PMCID: PMC3628721.

28. Langbaum JB, Fleisher AS, Chen K, Ayutyanont N, Lopera F, Quiroz YT, et al. Ushering in the study and treatment of preclinical Alzheimer disease. Nat Rev Neurol. 2013; 9(7):371–81. doi: 10.1038/nrneurol.2013.107 PMID: 23752908; PubMed Central PMCID: PMC4084675.

29. Reiman EM, Jagust WJ. Brain imaging in the study of Alzheimer's disease. Neuroimage. 2012; 61 (2):505–16. doi: 10.1016/j.neuroimage.2011.11.075 PMID: 22173295; PubMed Central PMCID: PMC3351556.

30. Fox NC, Scahill RI, Crum WR, Rossor MN. Correlation between rates of brain atrophy and cognitive decline in AD. Neurology. 1999; 52(8):1687–9. Epub 1999/05/20. PMID: 10331700.

31. Chen K, Reiman EM, Alexander GE, Caselli RJ, Gerkin R, Bandy D, et al. Correlations between apolipoprotein E epsilon4 gene dose and whole brain atrophy rates. Am J Psychiatry. 2007; 164(6):916–21. Epub 2007/06/02. 164/6/916 [pii] doi: 10.1176/appi.ajp.164.6.916 PMID: 17541051.

32. Stonnington CM, Chu C, Kloppel S, Jack CR Jr., Ashburner J, Frackowiak RS. Predicting clinical scores from magnetic resonance scans in Alzheimer's disease. Neuroimage. 2010; 51(4):1405–13. Epub 2010/03/30. S1053-8119(10)00338-1 [pii] doi: 10.1016/j.neuroimage.2010.03.051 PMID: 20347044; PubMed Central PMCID: PMC2871976.

33. Cardenas VA, Chao LL, Studholme C, Yaffe K, Miller BL, Madison C, et al. Brain atrophy associated with baseline and longitudinal measures of cognition. Neurobiol Aging. 2009. Epub 2009/05/19. S0197-4580(09)00139-0 [pii] doi: 10.1016/j.neurobiolaging.2009.04.011 PMID: 19446370.

34. Reiman EM, Uecker A, Caselli RJ, Lewis S, Bandy D, de Leon MJ, et al. Hippocampal volumes in cognitively normal persons at genetic risk for Alzheimer's disease. Ann Neurol. 1998; 44(2):288–91. Epub 1998/08/26. doi: 10.1002/ana.410440226 PMID: 9708558.

35. Thompson PM, Hayashi KM, de Zubicaray GI, Janke AL, Rose SE, Semple J, et al. Mapping hippocampal and ventricular change in Alzheimer's disease. NeuroImage. 2004; 22(4):1754–66. PMID: 15275931.

36. den Heijer T, van der Lijn F, Koudstaal PJ, Hofman A, van der Lugt A, Krestin GP, et al. A 10-year follow-up of hippocampal volume on magnetic resonance imaging in early dementia and cognitive decline. Brain. 2010; 133(4):1163–72. doi: 10.1093/brain/awq048 PMID: 20375138.

37. Wolz R, Heckemann RA, Aljabar P, Hajnal JV, Hammers A, Lötjönen J, et al. Measurement of hippocampal atrophy using 4D graph-cut segmentation: Application to ADNI. NeuroImage. 2010; 52 (1):109–18. PMID: 20382238. doi: 10.1016/j.neuroimage.2010.04.006

38. Jack CR Jr., Slomkowski M, Gracon S, Hoover TM, Felmlee JP, Stewart K, et al. MRI as a biomarker of disease progression in a therapeutic trial of milameline for AD. Neurology. 2003; 60(2):253–60. Epub 2003/01/29. PMID: 12552040; PubMed Central PMCID: PMC2745302.

39. Hua X, Lee S, Hibar DP, Yanovsky I, Leow AD, Toga AW, et al. Mapping Alzheimer's disease progression in 1309 MRI scans: Power estimates for different inter-scan intervals. NeuroImage. 2010; 51 (1):63–75. PMID: 20139010. doi: 10.1016/j.neuroimage.2010.01.104

40. Wang Y, Song Y, Rajagopalan P, An T, Liu K, Chou YY, et al. Surface-based TBM boosts power to detect disease effects on the brain: An N = 804 ADNI study. Neuroimage. 2011; 56(4):1993–2010. Epub 2011/03/29. S1053-8119(11)00318-1 [pii] doi: 10.1016/j.neuroimage.2011.03.040 PMID: 21440071.

41. Shi J, Stonnington CM, Thompson PM, Chen K, Gutman B, Reschke C, et al. Studying ventricular abnormalities in mild cognitive impairment with hyperbolic Ricci flow and tensor-based morphometry. Neuroimage. 2015; 104:1–20. doi: 10.1016/j.neuroimage.2014.09.062 PMID: 25285374; PubMed Central PMCID: PMC4252650.

42. de Leon MJ, George AE, Stylopoulos LA, Smith G, Miller DC. Early marker for Alzheimer's disease: the atrophic hippocampus. Lancet. 1989; 2(8664):672–3. PMID: 2570916.

43. Jack CR Jr., Shiung MM, Gunter JL, O'Brien PC, Weigand SD, Knopman DS, et al. Comparison of different MRI brain atrophy rate measures with clinical disease progression in AD. Neurology. 2004; 62 (4):591–600. PMID: 14981176; PubMed Central PMCID: PMC2730165.

44. Wang Y, Zhang J, Gutman B, Chan TF, Becker JT, Aizenstein HJ, et al. Multivariate tensor-based morphometry on surfaces: Application to mapping ventricular abnormalities in HIV/AIDS. NeuroImage. 2010; 49(3):2141–57. Epub 2009/11/11. S1053-8119(09)01158-6 [pii] doi: 10.1016/j.neuroimage.2009.10.086 PMID: 19900560.

45. Wang Y, Shi J, Yin X, Gu X, Chan TF, Yau S-T, et al. Brain Surface Conformal Parameterization with the Ricci Flow. IEEE Trans Med Imag. 2012; 31(2):251–64. PMID: 21926017.

46. Shi J, Thompson PM, Gutman B, Wang Y. Surface fluid registration of conformal representation: Application to detect disease burden and genetic influence on hippocampus. Neuroimage. 2013; 78C:111–34. Epub 2013/04/17. doi: 10.1016/j.neuroimage.2013.04.018 PMID: 23587689.

47. Shi J, Wang Y, Ceschin R, An X, Lao Y, Vanderbilt D, et al. A Multivariate Surface-Based Analysis of the Putamen in Premature Newborns: Regional Differences within the Ventral Striatum. PLoS One. 2013; 8(7):e66736. Epub 2013/07/12. doi: 10.1371/journal.pone.0066736 PMID: 23843961; PubMed Central PMCID: PMC3700976.

48. Folstein MF, Folstein SE, McHugh PR. "Mini-mental state". A practical method for grading the cognitive state of patients for the clinician. J Psychiatr Res. 1975; 12(3):189–98. Epub 1975/11/01. 0022-3956(75)90026-6 [pii]. PMID: 1202204.

49. Berg L. Clinical Dementia Rating (CDR). Psychopharmacol Bull. 1988; 24(4):637–9. Epub 1988/01/01. PMID: 3249765.

50. Wechsler D. Wechsler Memory Scale-Revised Manual. San Antonio, TX: Psychological Corporation; 1987.

51. Jack CR Jr., Bernstein MA, Fox NC, Thompson P, Alexander G, Harvey D, et al. The Alzheimer's disease neuroimaging initiative (ADNI): MRI methods. Journal of Magnetic Resonance Imaging. 2008; 27(4):685–91. PMID: 18302232; PubMed Central PMCID: PMCPMC2544629. doi: 10.1002/jmri.21049

52. Morra JH, Tu Z, Apostolova LG, Green AE, Avedissian C, Madsen SK, et al. Automated 3D mapping of hippocampal atrophy and its clinical correlates in 400 subjects with Alzheimer's disease, mild cognitive impairment, and elderly controls. Hum Brain Mapp. 2009; 30(9):2766–88. Epub 2009/01/28. doi: 10.1002/hbm.20708 PMID: 19172649; PubMed Central PMCID: PMC2733926.

53. Patenaude B, Smith SM, Kennedy DN, Jenkinson M. A Bayesian model of shape and appearance for subcortical brain segmentation. Neuroimage. 2011; 56(3):907–22. Epub 2011/03/01. doi: 10.1016/j.neuroimage.2011.02.046 PMID: 21352927.

54. Wang Y, Lui LM, Gu X, Hayashi KM, Chan TF, Toga AW, et al. Brain Surface Conformal Parameterization using Riemann Surface Structure. IEEE Trans Med Imag. 2007; 26(6):853–65. PMID: 17679336.

55. Wang Y, Yuan L, Shi J, Greve A, Ye J, Toga AW, et al. Applying tensor-based morphometry to parametric surfaces can improve MRI-based disease diagnosis. Neuroimage. 2013; 74:209–30. Epub 2013/02/26. doi: 10.1016/j.neuroimage.2013.02.011 PMID: 23435208; PubMed Central PMCID: PMC3641904.

56. Lao Y, Wang Y, Shi J, Ceschin R, Nelson MD, Panigrahy A, et al. Thalamic alterations in preterm neonates and their relation to ventral striatum disturbances revealed by a combined shape and pose analysis. Brain Struct Funct. 2014. doi: 10.1007/s00429-014-0921-7 PMID: 25366970.

57. Joshi SH, Espinoza RT, Pirnia T, Shi J, Wang Y, Ayers B, et al. Structural plasticity of the hippocampus and amygdala induced by electroconvulsive therapy in major depression. Biological Psychiatry. 2015. doi: 10.1016/j.biopsych.2015.02.029

58. Lorensen WE, Cline HE. Marching cubes: A high resolution 3D surface construction algorithm. SIGGRAPH Comput Graph. 1987; 21(4):163–9. doi: 10.1145/37402.37422

59. Bro-Nielsen M, Gramkow C. Fast fluid registration of medical images. Visualization in Biomedical Computing (VBC'96) Springer; 1996. p. 267–76.

60. D'Agostino E, Maes F, Vandermeulen D, Suetens P. A viscous fluid model for multimodal non-rigid image registration using mutual information. Med Image Anal. 2003; 7(4):565–75. Epub 2003/10/17. PMID: 14561559.

61. Rey D, Subsol G, Delingette H, Ayache N. Automatic detection and segmentation of evolving processes in 3D medical images: Application to multiple sclerosis. Med Image Anal. 2002; 6(2):163–79. Epub 2002/06/05. S1361841502000567 [pii]. PMID: 12045002.

62. Leow A, Huang SC, Geng A, Becker J, Davis S, Toga A, et al. Inverse consistent mapping in 3D deformable image registration: its construction and statistical properties. Inf Process Med Imaging. 2005; 19:493–503. Epub 2007/03/16. PMID: 17354720.

63. Pizer S, Fritsch D, Yushkevich P, Johnson V, Chaney E. Segmentation, registration, and measurement of shape variation via image object shape. IEEE Trans Med Imag. 1999; 18:851–65. PMID: 10628945.

64. Arsigny V, Fillard P, Pennec X, Ayache N. Log-Euclidean Metrics for Fast and Simple Calculus on Diffusion Tensors. Magn Reson Med. 2006; 56(2):411–21. PMID: 16788917.

65. Hotelling H. The generalization of Student's ratio. Ann Math Statist. 1931; 2:360–78.

66. Cao J, Worsley KJ. The detection of local shape changes via the geometry of Hotelling's T^2 fields. Ann Statist. 1999; 27(3):925–42.

67. Thirion JP, Prima S, Subsol G, Roberts N. Statistical analysis of normal and abnormal dissymmetry in volumetric medical images. Med Image Anal. 2000; 4(2):111–21. PMID: 10972325

68. Kim WH, Pachauri D, Hatt C, Chung MK, Johnson SC, Singh V, editors. Wavelet based multi-scale shape features on arbitrary surfaces for cortical thickness discrimination. Advances in Neural Information Processing Systems (NIPS) 2012.

69. Leporé N, Brun C, Chou Y-Y, Chiang M-C, Dutton RA, Hayashi KM, et al. Generalized Tensor-Based Morphometry of HIV/AIDS Using Multivariate Statistics on Deformation Tensors. IEEE Trans Med Imag. 2008; 27(1):129–41. PMID: 18270068.

70. Holmes AP, Blair RC, Watson JD, Ford I. Nonparametric analysis of statistic images from functional mapping experiments. J Cereb Blood Flow Metab. 1996; 16(1):7–22. Epub 1996/01/01. doi: 10.1097/00004647-199601000-00002 PMID: 8530558.

71. Nichols TE, Holmes AP. Nonparametric permutation tests for functional neuroimaging: a primer with examples. Hum Brain Mapp. 2002; 15(1):1–25. Epub 2001/12/18. doi: 10.1002/hbm.1058 [pii]. PMID: 11747097.

72. Zannis VI, Breslow JL. Apolipoprotein E. Mol Cell Biochem. 1982; 42(1):3–20. PMID: 7038438.

73. Zannis VI, Breslow JL, Utermann G, Mahley RW, Weisgraber KH, Havel RJ, et al. Proposed nomenclature of apoE isoproteins, apoE genotypes, and phenotypes. J Lipid Res. 1982; 23(6):911–4. PMID: 7130859.

74. Corder EH, Saunders AM, Risch NJ, Strittmatter WJ, Schmechel DE, Gaskell PC Jr., et al. Protective effect of apolipoprotein E type 2 allele for late onset Alzheimer disease. Nat Genet. 1994; 7(2):180–4. doi: 10.1038/ng0694-180 PMID: 7920638.

75. Blacker D, Lee H, Muzikansky A, Martin EC, Tanzi R, McArdle JJ, et al. Neuropsychological measures in normal individuals that predict subsequent cognitive decline. Arch Neurol. 2007; 64(6):862–71. doi: 10.1001/archneur.64.6.862 PMID: 17562935.

76. Benjamini Y, Hochberg Y. Controlling the False Discovery Rate: A Practical and Powerful Approach to Multiple Testing. Journal of the Royal Statistical Society Series B (Methodological). 1995; 57 (1):289–300. citeulike-article-id:1042553.

77. Wang G, Zhang X, Su Q, Shi J, Caselli RJ, Wang Y, et al. A novel cortical thickness estimation method based on volumetric Laplace-Beltrami operator and heat kernel. Med Image Anal. 2015; 22(1):1–20. doi: 10.1016/j.media.2015.01.005 PMID: 25700360.

78. Pievani M, Galluzzi S, Thompson PM, Rasser PE, Bonetti M, Frisoni GB. APOE4 is associated with greater atrophy of the hippocampal formation in Alzheimer's disease. Neuroimage. 2011; 55(3):909–19. Epub 2011/01/13. S1053-8119(11)00005-X [pii] doi: 10.1016/j.neuroimage.2010.12.081 PMID: 21224004.

79. Soininen H, Partanen K, Pitkanen A, Hallikainen M, Hanninen T, Helisalmi S, et al. Decreased hippocampal volume asymmetry on MRIs in nondemented elderly subjects carrying the apolipoprotein E epsilon 4 allele. Neurology. 1995; 45(2):391–2. PMID: 7854548.

80. Lemaitre H, Crivello F, Dufouil C, Grassiot B, Tzourio C, Alperovitch A, et al. No epsilon4 gene dose effect on hippocampal atrophy in a large MRI database of healthy elderly subjects. Neuroimage. 2005; 24(4):1205–13. Epub 2005/01/27. S1053-8119(04)00618-4 [pii] doi: 10.1016/j.neuroimage.2004.10.016 PMID: 15670698.

81. Crivello F, Lemaitre H, Dufouil C, Grassiot B, Delcroix N, Tzourio-Mazoyer N, et al. Effects of ApoE-epsilon4 allele load and age on the rates of grey matter and hippocampal volumes loss in a longitudinal cohort of 1186 healthy elderly persons. Neuroimage. 2010; 53(3):1064–9. doi: 10.1016/j.neuroimage.2009.12.116 PMID: 20060049.

82. Protas HD, Chen K, Langbaum JB, Fleisher AS, Alexander GE, Lee W, et al. Posterior cingulate glucose metabolism, hippocampal glucose metabolism, and hippocampal volume in cognitively normal, late-middle-aged persons at 3 levels of genetic risk for Alzheimer disease. JAMA Neurol. 2013; 70 (3):320–5. doi: 10.1001/2013.jamaneurol.286 PMID: 23599929; PubMed Central PMCID: PMC3745014.

83. Lyall DM, Royle NA, Harris SE, Bastin ME, Maniega SM, Murray C, et al. Alzheimer's disease susceptibility genes APOE and TOMM40, and hippocampal volumes in the Lothian birth cohort 1936. PLoS One. 2013; 8(11):e80513. doi: 10.1371/journal.pone.0080513 PMID: 24260406; PubMed Central PMCID: PMC3829876.

84. Cohen RM, Small C, Lalonde F, Friz J, Sunderland T. Effect of apolipoprotein E genotype on hippocampal volume loss in aging healthy women. Neurology. 2001; 57(12):2223–8. PMID: 11756601.

85. O'Dwyer L, Lamberton F, Matura S, Tanner C, Scheibe M, Miller J, et al. Reduced hippocampal volume in healthy young ApoE4 carriers: an MRI study. PLoS One. 2012; 7(11):e48895. doi: 10.1371/journal.pone.0048895 PMID: 23152815; PubMed Central PMCID: PMC3494711.

86. Farrer LA, Cupples LA, Haines JL, Hyman B, Kukull WA, Mayeux R, et al. Effects of age, sex, and ethnicity on the association between apolipoprotein E genotype and Alzheimer disease. A meta-analysis. APOE and Alzheimer Disease Meta Analysis Consortium. JAMA. 1997; 278(16):1349–56. Epub 1997/10/29. PMID: 9343467.

87. de Flores R, La Joie R, Landeau B, Perrotin A, Mezenge F, de La Sayette V, et al. Effects of age and Alzheimer's disease on hippocampal subfields: comparison between manual and FreeSurfer volumetry. Hum Brain Mapp. 2015; 36(2):463–74. doi: 10.1002/hbm.22640 PMID: 25231681.

88. Hao Y, Wang T, Zhang X, Duan Y, Yu C, Jiang T, et al. Local label learning (LLL) for subcortical structure segmentation: application to hippocampus segmentation. Hum Brain Mapp. 2014; 35(6):2674–97. doi: 10.1002/hbm.22359 PMID: 24151008.

89. Wang L, Swank JS, Glick IE, Gado MH, Miller MI, Morris JC, et al. Changes in hippocampal volume and shape across time distinguish dementia of the Alzheimer type from healthy aging. NeuroImage. 2003; 20(2):667–82. PMID: 14568443.

90. Wang L, Miller JP, Gado MH, McKeel DW, Rothermich M, Miller MI, et al. Abnormalities of hippocampal surface structure in very mild dementia of the Alzheimer type. Neuroimage. 2006; 30(1):52–60. Epub 2005/10/26. S1053-8119(05)00716-0 [pii] doi: 10.1016/j.neuroimage.2005.09.017 PMID: 16243546; PubMed Central PMCID: PMC2853193.

91. Van Leemput K, Bakkour A, Benner T, Wiggins G, Wald LL, Augustinack J, et al. Automated segmentation of hippocampal subfields from ultra-high resolution in vivo MRI. Hippocampus. 2009; 19

(6):549–57. Epub 2009/05/01. doi: 10.1002/hipo.20615 PMID: 19405131; PubMed Central PMCID: PMC2739884.

92. Yassa MA, Stark SM, Bakker A, Albert MS, Gallagher M, Stark CE. High-resolution structural and functional MRI of hippocampal CA3 and dentate gyrus in patients with amnestic Mild Cognitive Impairment. Neuroimage. 2010; 51(3):1242–52. Epub 2010/03/27. doi: 10.1016/j.neuroimage.2010.03.040 PMID: 20338246; PubMed Central PMCID: PMC2909476.

93. Yushkevich PA, Amaral RS, Augustinack JC, Bender AR, Bernstein JD, Boccardi M, et al. Quantitative comparison of 21 protocols for labeling hippocampal subfields and parahippocampal subregions in in vivo MRI: Towards a harmonized segmentation protocol. Neuroimage. 2015. doi: 10.1016/j.neuroimage.2015.01.004 PMID: 25596463.

94. Yushkevich PA, Pluta JB, Wang H, Xie L, Ding SL, Gertje EC, et al. Automated volumetry and regional thickness analysis of hippocampal subfields and medial temporal cortical structures in mild cognitive impairment. Hum Brain Mapp. 2015; 36(1):258–87. doi: 10.1002/hbm.22627 PMID: 25181316; PubMed Central PMCID: PMC4313574.

95. Brechbühler C, Gerig G, Kübler O. Parametrization of Closed Surfaces for 3-D Shape Description. Computer Vision and Image Understanding. 1995; 61(2):154–70. doi: 10.1006/cviu.1995.1013

96. Gu X, Wang Y, Chan TF, Thompson PM, Yau S-T. Genus zero surface conformal mapping and its application to brain surface mapping. IEEE Trans Med Imag. 2004; 23(8):949–58. PMID: 15338729.

97. Styner M, Lieberman JA, Pantazis D, Gerig G. Boundary and medial shape analysis of the hippocampus in schizophrenia. Med Image Anal. 2004; 8(3):197–203. Epub 2004/09/29. doi: 10.1016/j.media.2004.06.004 PMID: 15450215.

98. Shen L, Firpi HA, Saykin AJ, West JD. Parametric surface modeling and registration for comparison of manual and automated segmentation of the hippocampus. Hippocampus. 2009; 19(6):588–95. Epub 2009/05/01. doi: 10.1002/hipo.20613 PMID: 19405146; PubMed Central PMCID: PMC2849649.

99. Gutman B, Wang Y, Morra J, Toga AW, Thompson PM. Disease classification with hippocampal shape invariants. Hippocampus. 2009; 19(6):572–8. PMID: 19437498. doi: 10.1002/hipo.20627

100. Csernansky JG, Wang L, Joshi S, Miller JP, Gado M, Kido D, et al. Early DAT is distinguished from aging by high-dimensional mapping of the hippocampus. Dementia of the Alzheimer type. Neurology. 2000; 55(11):1636–43. Epub 2000/12/13. PMID: 11113216.

101. Wang L, Beg F, Ratnanather T, Ceritoglu C, Younes L, Morris JC, et al. Large deformation diffeomorphism and momentum based hippocampal shape discrimination in dementia of the Alzheimer type. IEEE Trans Med Imaging. 2007; 26(4):462–70. Epub 2007/04/13. doi: 10.1109/TMI.2005.853923 PMID: 17427733; PubMed Central PMCID: PMC2848689.

102. Joshi SC, Miller MI. Landmark matching via large deformation diffeomorphisms. IEEE Trans Image Process. 2000; 9(8):1357–70. Epub 2008/02/12. doi: 10.1109/83.855431 PMID: 18262973.

103. Haller JW, Christensen GE, Joshi SC, Newcomer JW, Miller MI, Csernansky JG, et al. Hippocampal MR imaging morphometry by means of general pattern matching. Radiology. 1996; 199(3):787–91. Epub 1996/06/01. PMID: 8638006.

104. Apostolova LG, Morra JH, Green AE, Hwang KS, Avedissian C, Woo E, et al. Automated 3D mapping of baseline and 12-month associations between three verbal memory measures and hippocampal atrophy in 490 ADNI subjects. Neuroimage. 2010; 51(1):488–99. Epub 2010/01/20. doi: 10.1016/j.neuroimage.2009.12.125 PMID: 20083211; PubMed Central PMCID: PMC2847034.

105. Cho Y, Seong JK, Shin SY, Jeong Y, Kim JH, Qiu A, et al. A multi-resolution scheme for distortion-minimizing mapping between human subcortical structures based on geodesic construction on Riemannian manifolds. Neuroimage. 2011; 57(4):1376–92. Epub 2011/06/11. S1053-8119(11)00574-X [pii] doi: 10.1016/j.neuroimage.2011.05.066 PMID: 21658456.

106. Kim S-G, Chung MK, Schaefer SM, van Reekum C, Davidson RJ. Sparse Shape Representation using the Laplace-Beltrami Eigenfunctions and Its Application to Modeling Subcortical Structures. Proceedings / sponsored by IEEE Computer Society Technical Committee on Pattern Analysis and Machine Intelligence Workshop on Mathematical Methods in Biomedical Image Analysis. 2012:25–32. doi: 10.1109/MMBIA.2012.6164736. PMC3684562.

107. Wachinger C, Golland P, Kremen W, Fischl B, Reuter M, Alzheimer's Disease Neuroimaging I. BrainPrint: A discriminative characterization of brain morphology. Neuroimage. 2015; 109:232–48. doi: 10.1016/j.neuroimage.2015.01.032 PMID: 25613439; PubMed Central PMCID: PMC4340729.

108. Yang X, Goh A, Chen SH, Qiu A. Evolution of hippocampal shapes across the human lifespan. Hum Brain Mapp. 2013; 34(11):3075–85. doi: 10.1002/hbm.22125 PMID: 22815197.

109. Younes L, Ratnanather JT, Brown T, Aylward E, Nopoulos P, Johnson H, et al. Regionally selective atrophy of subcortical structures in prodromal HD as revealed by statistical shape analysis. Hum

Brain Mapp. 2014; 35(3):792–809. doi: 10.1002/hbm.22214 PMID: 23281100; PubMed Central PMCID: PMC3715588.

110. Li B, Mcmahon T, Shi J, Gutman BA, Thompson PM, Baxter LC, et al. Correlation between ApoE4 Genotype and Hippocampal Atrophy on Arizona APOE Cohort: A Surface Multivariate Tensor-based Morphometry Study Arizona Alzheimer's Consortium Annual Scientific Conference; Tempe, AZ2015.

111. Zhang W, Shi J, Chen K, Baxter LC, Reiman EM, Caselli RJ, et al. An Automatic Surface-based Ventricular Morphometry Pipeline and Its Application in Alzheimer's Disease Research. Arizona Alzheimer's Consortium Annual Scientific Conference; Tempe, AZ2015.